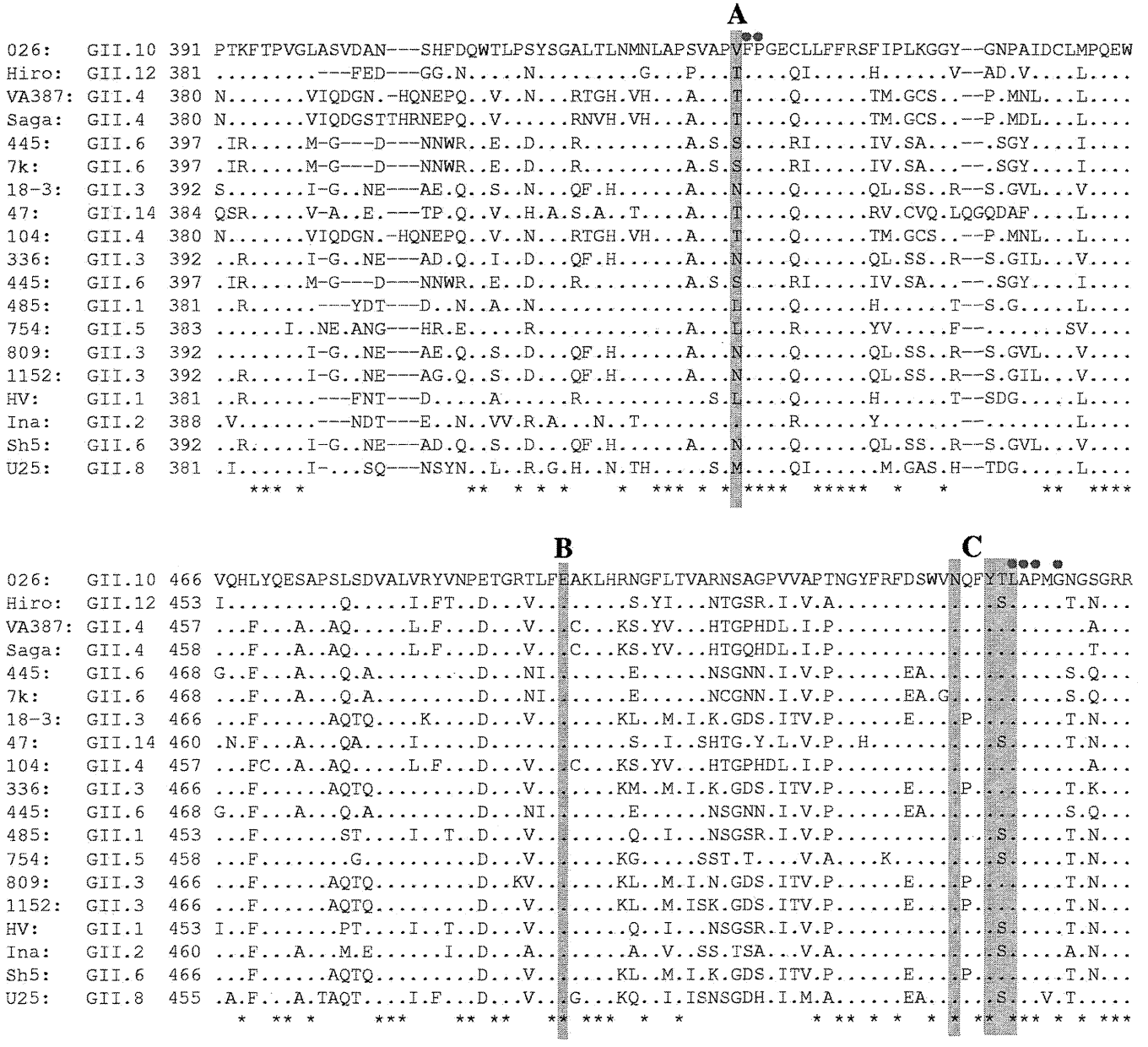


FIG 3 Amino acid alignment of GII capsid sequences indicated that four GII.10 P domain residues involved in binding 5B18 Fab were highly conserved among other GII genotypes. Ten different GII genotypes' capsid sequences were aligned (strain name is followed by genotype), and the GII.10 capsid sequence was used as the consensus (21). The GII.10 P domain residues that interacted with the 5B18 Fab involved three different sites on the P domain, termed A, B, and C. The blue shading shows the six GII.10 P domain residues that interacted with the 5B18 Fab, and from the alignment, four of six residues were highly conserved among other GII genotypes. The red circles show the suspected binding site of MAb14-1 monoclonal antibody (59).

Together, these results suggest that 5B18 appears capable of detecting nominally intact GII.10 VLPs.

**Norovirus variability and 5B18 detection.** As stated previously, norovirus displays considerable genetic variation. Mapping this variation onto the VLP structure shows that this variation is concentrated on the outer surface of the virion, with buried portions of the P and S domains being much more conserved (Fig. 7). If one were only able to access the outer surface of the VLP, this genetic variation would make pan-recognition extremely difficult. The 5B18 mode of recognition thus provides a mechanism to achieve broad VLP detection by recognizing a conserved surface that is transiently exposed in a dynamic manner. Indeed, the Fab footprint was highly conserved on the GII P domains (Fig. 7C).

## DISCUSSION

Human noroviruses are genetically and antigenically distinct, but broad-range monoclonal antibodies capable of detecting multiple norovirus genogroups and genotypes have been described (21, 39, 40, 50, 59, 70). One such antibody, 5B18, is currently in use in a commercial norovirus ELISA detection kit (Denka Seiken, Japan) and was found to bind to numerous GII genotypes but not GI noroviruses (unpublished data). To describe the precise binding

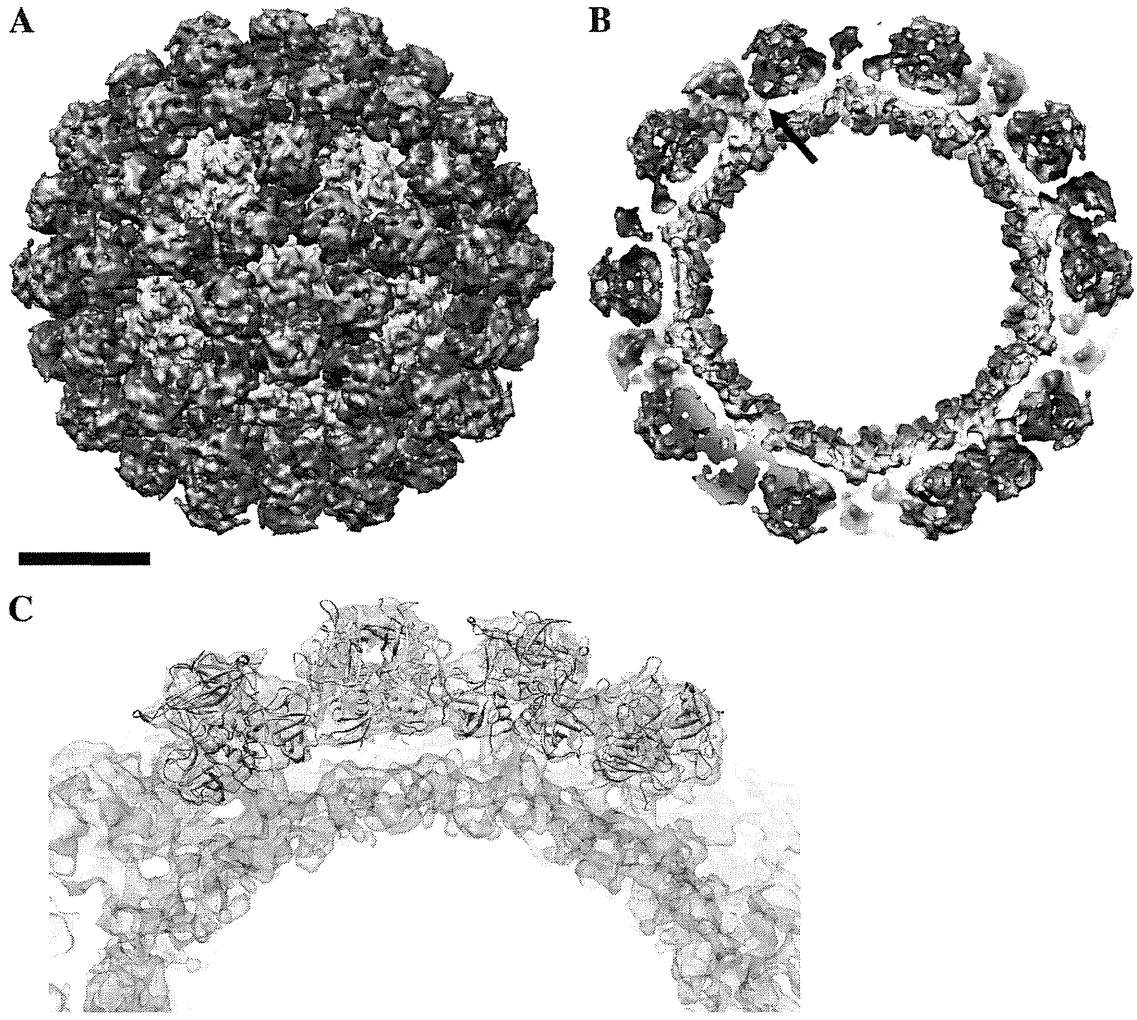


FIG 4 The cryo-EM structure of the GII.10 VLP consisted of an S domain surrounded by 90 P domain dimers. (A) The GII.10 S domain was surface exposed (yellow and yellow to green). The P domain dimers (green to blue and purple) were raised off the S domain by ~15 Å. (B) The inner surface of the S domain is colored red. The S domain was connected to the P domain monomer by a narrow hinge region (single arrow; the other hinges were not labeled for clarity). The scale bar for panels A and B indicates 100 Å. (C) Fitting and modeling of the GII.10 P domain (apo P domain structure) into the A/B dimer subunit (light blue and pink, respectively) and C/C dimer subunit (cyan).

location of 5B18, we determined the X-ray crystal structure of the GII.10 P domain-Fab complex. We also determined the cryo-EM structure of the GII.10 VLPs in an attempt to understand the 5B18 Fab binding interaction in the context of the entire virus particle.

The 5B18 Fab binds to a face of the GII.10 P1 subdomain close to the S domain and not openly exposed at the VLP surface. Six amino acid residues on the P1 subdomain make main chain and side chain interactions with the Fab. Four of these residues are highly conserved among numerous GII norovirus genotypes (Fig. 3). Variation at these residues appears to be tolerated, as the 5B18 antibody detects both GII.4 VLPs, which had Thr433 (instead of Val433), and GII.12 VLPs, which had Thr433 and Ser534 (instead of Val433 and Thr534, respectively). Surprisingly, the 5B18 Fab contact residues are almost identical to those of another broad-range monoclonal antibody, MAb14-1 (Fig. 3) (59). Furthermore, the epitopes of two other broad-range monoclonal antibodies, NV3901 and NV3912, are in this general region (50). The MAb14-1 antibody was shown to bind VLPs from many GII genotypes and several GI genotypes, including a GI.1 genotype, whereas the NV3901 and NV3912 antibodies were found to only bind GI genotypes. Interestingly, the 5B18, MAb14-1, and NV3901/NV3912 antibodies were raised in different mice immunized with different VLPs and their binding sites were all in close proximity on the P1 subdomain (50). Although the precise structural binding details of MAb14-1, NV3901, and NV3912 antibodies have not been described, it suggests that the P1 subdomain was an important antigenic site for GI and GII noroviruses. Moreover, the P1 subdomain likely contained GI and GII cross-reactive epitopes. Superpositioning of published X-ray crystal structures of norovirus P domain (GI.1, GII.4, GII.9, GII.12, and GV.1) onto the GII.10 P domain-Fab complex structure showed that three of six amino acids involved in the 5B18 Fab binding were highly conserved for three norovirus genogroups and that the conformation of their side chains closely resembles those of GII.10 (see Table S2 and Fig. S4 in the supplemental material). Taken together, the results indicate that the 5B18 binding epitope represents an important site for antibody recognition (Fig. 7).

Initially, the X-ray crystal structure of the GI.1 VLP (53) was

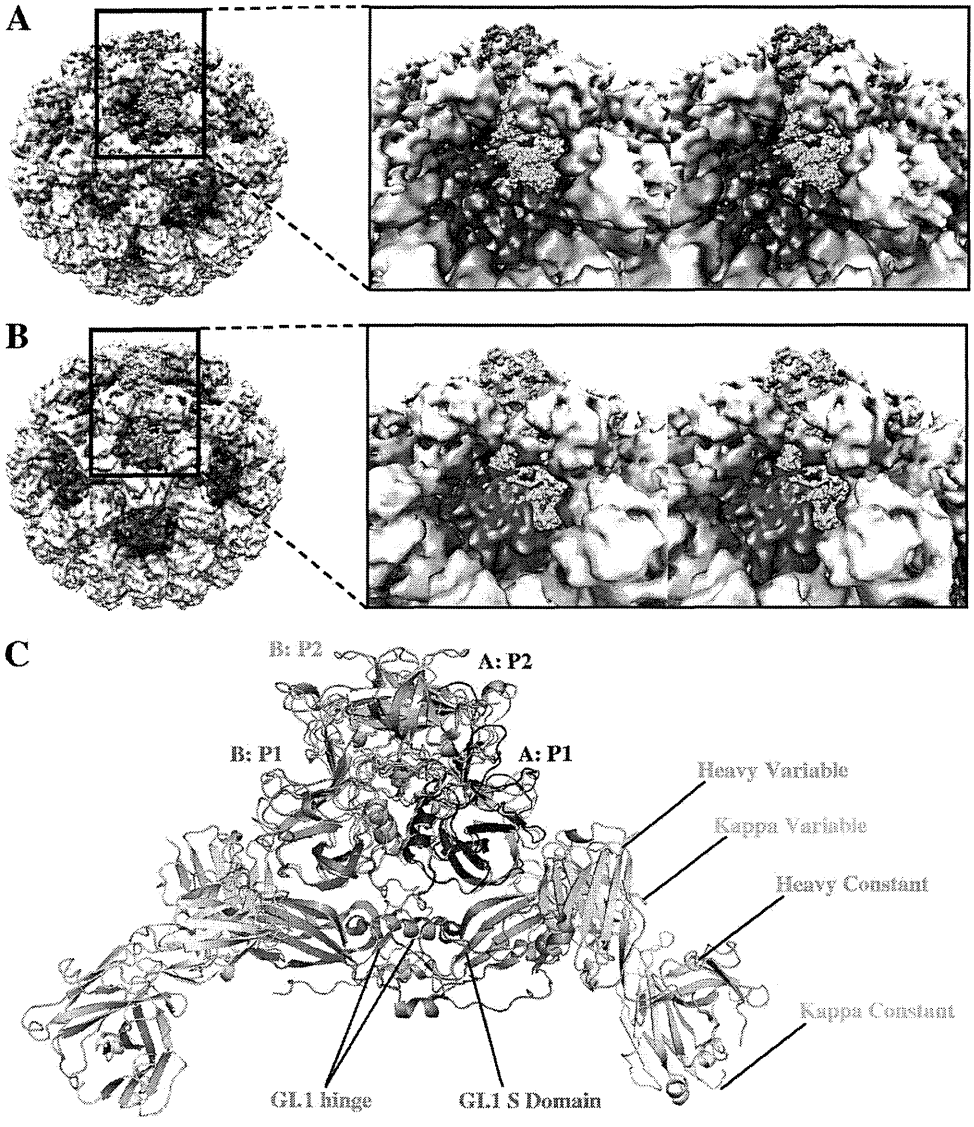


FIG 5 The X-ray crystal structure of the GII.10 P domain-Fab complex fitted into the cryo-EM structure of the GII.10 VLP and the X-ray crystal structure of the GI.1 VLP (PDB ID 1IHM). (A) The P domain (light blue and pink) from the P domain-Fab was fitted into the A/B dimer subunit on the VLP. The boxed region shows a close-up stereoview of the interaction. The Fab appeared to make slight contact with the S domain at the space at the 6-fold axes and was under a neighboring domain. (B) The P domain (cyan) from the P domain-Fab was fitted into the C/C dimer subunit on the VLP. The boxed region shows a close-up stereoview of the interaction. The Fab appeared to make contact with a raised S domain structure at the space at the 5-fold axes and was for the most part hidden under a neighboring domain. (C) The GII.10 P domain (colored as in Fig. 1 and rotated 90° from the views in Fig. 5A and 5B) was highly similar to the GI.1 P domain (light gray), but the Fabs clashed with the GI.1 S domain (orange).

used for fitting the GII.10 P domain-Fab complex and to describe the binding interaction in the context of the entire particle. The P domains of GI.1 and GII.10 matched well (root mean square deviation [RMSD], 1.3 Å), but the 5B18 Fab clashed with the GI.1 S domain (Fig. 5C). Indeed, the P domains in GI.1 VLPs rest on the S domains, and this necessarily placed most of the Fab structure into a position that overlapped the S domain (Fig. 5C). In an attempt to understand the 5B18 antibody interaction in the context of a GII VLP, the cryo-EM structure of the GII.10 VLP was determined to an ~10-Å resolution. Recent cryo-EM studies have shown that GI.1 and GV.1 norovirus capsid structures are strikingly different (30, 67), whereas another study indicated that GI.1 and GII.4 (Grimsby virus) capsids are highly similar (12). The cryo-EM structure of the GII.10 VLPs showed several structural similarities to the GV.1 virion, including a raised P domain, P1-P1 subdomain contacts, and an extended hinge region (see Fig. S6 in the supplemental material). In addition, the GII.10 and GV.1 P domain dimers were rotated ~40° clockwise compared to the orientation of the GI.1 P domain dimer (data not shown). Fitting of the X-ray crystal structure of the GII.10 P domain-Fab complex into the GII.10 VLP structure showed that the P domain could be positioned unambiguously into the P domain density of the EM map; however, this placement resulted in significant overlap between Fab and neighboring P and S domains in the virus particle (Fig. 5). One potential explanation for this result is that the VLPs flexibly expose the P domain to the 5B18 antibody by rotating the

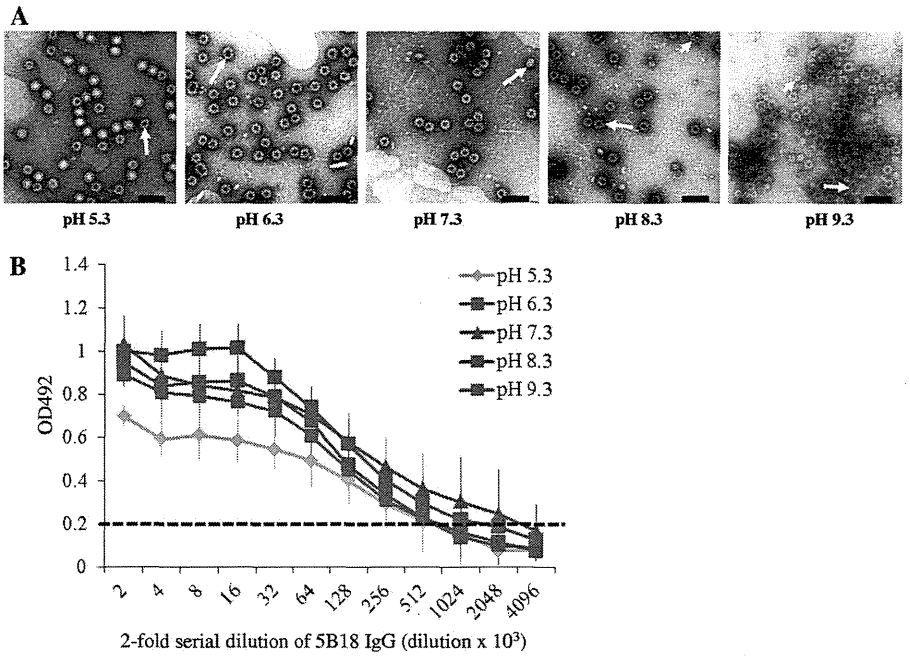


FIG 6 An antibody ELISA was used to determine the binding ability of IgG to GII.10 VLPs. (A) The morphology of the VLPs was examined using EM. At low pHs (from pH 5.3 to 7.3), the majority of the VLPs appeared intact, while above pH 7.3, many of the VLPs appeared broken (long arrows). Small VLPs were also found (short arrows). Scale bar, 100 nm. (B) The same VLPs shown in panel A were used in an ELISA to compare the binding ability of 5B18 IgG. The OD values represent the means of the results for 4 wells; error bars are shown. The OD at 492 nm (OD492) was determined; the dashed line shows the OD492 cutoff of 0.2 (21). The 5B18 IgG detected GII.10 VLPs at different pH values. At pH 7.3, the titer was 2,048,000, while the titers of the other pH values were 2- or 4-fold lower, indicating similar cross-reactivities.

P domains out of the conformation observed in the cryo-EM reconstruction and breaking the P1-P1 domain contacts seen in the VLP. This may be possible since the S domain-P1 subdomain connection in GII noroviruses is particularly long and flexible.

The structural differences between the GI.1 and GII.10 norovirus VLPs do not appear to be a consequence of sequence diversity, since the GI.1 and GII.4 VLP structures are similar and distinct from the GV.1 virion and GII.10 VLP structures. Moreover, the VLP preparation and cryo-EM techniques appear to be essentially the same (54). Two factors that may have affected the particle structures were the insect cell type and the pH of the VLPs. The GI.1 VLPs were expressed in *Spodoptera frugiperda* (Sf9) cells, purified by CsCl ultracentrifugation, and then resuspended in water (pH not described in text) (53, 54), and the GII.10 VLPs were expressed in *Trichopulsia ni* (H5) cells, purified by CsCl ultracentrifugation, and then resuspended in PBS (pH 7.3). We note parenthetically that the cryo-EM structures of hepatitis E virus VLPs expressed in Sf9 and H5 cells are similar, although the processing of the viral protein appeared different (38). Our EM results showed that GII.10 VLPs were intact particles at pH 5.3, 6.3, and 7.3, while another study found that the diameter of norovirus VLPs remained virtually unchanged at pH 3 to 7 but appeared smaller at pH 8 (2). This suggests that the insect cell line and water/PBS (neutral pH) did not affect the overall structure of the VLPs. However, another study has shown that a pH change from 7.6 to 5.0 could cause large structural changes in *Nudaurelia capensis* ω virus VLPs (43, 62). It is possible that these varied conformations do not represent different, stable norovirus structures but are rather all part of a wide spectrum of conformations afforded by the flexible tether between the P and S domains. From previous studies (30), it is clear that this "floating P domain" conformation is independent of whether the sample is a VLP or infectious virion. Since this extended conformation is now observed in rabbit hemorrhagic disease virus (also a calicivirus, genus *Lagovirus*), it also cannot be dependent upon calicivirus genera. It is possible that the energy differences between the conformations represented by these viruses is relatively small and that subtle protein-protein interaction differences favor one conformation under particular conditions. It would be particularly interesting to examine the conformations of these viruses under a broad range of conditions that mimic the expected environments during the viral life cycle. Such changes in virion structure have been observed with numerous other viruses (3, 9, 46, 64, 71). In the case of GV.1 norovirus, where there is an animal model (69) and infectious clone (66), it would also be important to determine what role this flexible tether region has in the replication of the virions and pathology of the disease.

It is important to note that the observed ELISA binding of 5B18 IgG may not occur with intact VLPs. It is possible that denatured or partially broken VLPs or the presence of contaminating GII.10 VP1 was responsible for the binding observed in the ELISA (19, 20, 24). However, it is known that high pH (8.3 or above), partially breaks or denatures norovirus VLPs (2). Despite this pH dependence, the titer remained almost identical, especially in the comparison between pHs 7.3 to 9.3 (Fig. 6), suggesting that only intact or structurally stable virions are being detected. Moreover, the 5B18 antibody could detect GII.10 VLPs that were bound to the plates via histo-blood group antigens, which required a dimeric interaction (22; also unpublished data). Finally three other antibodies, MAb14-1 and NV3901/NV3912, which bound in close

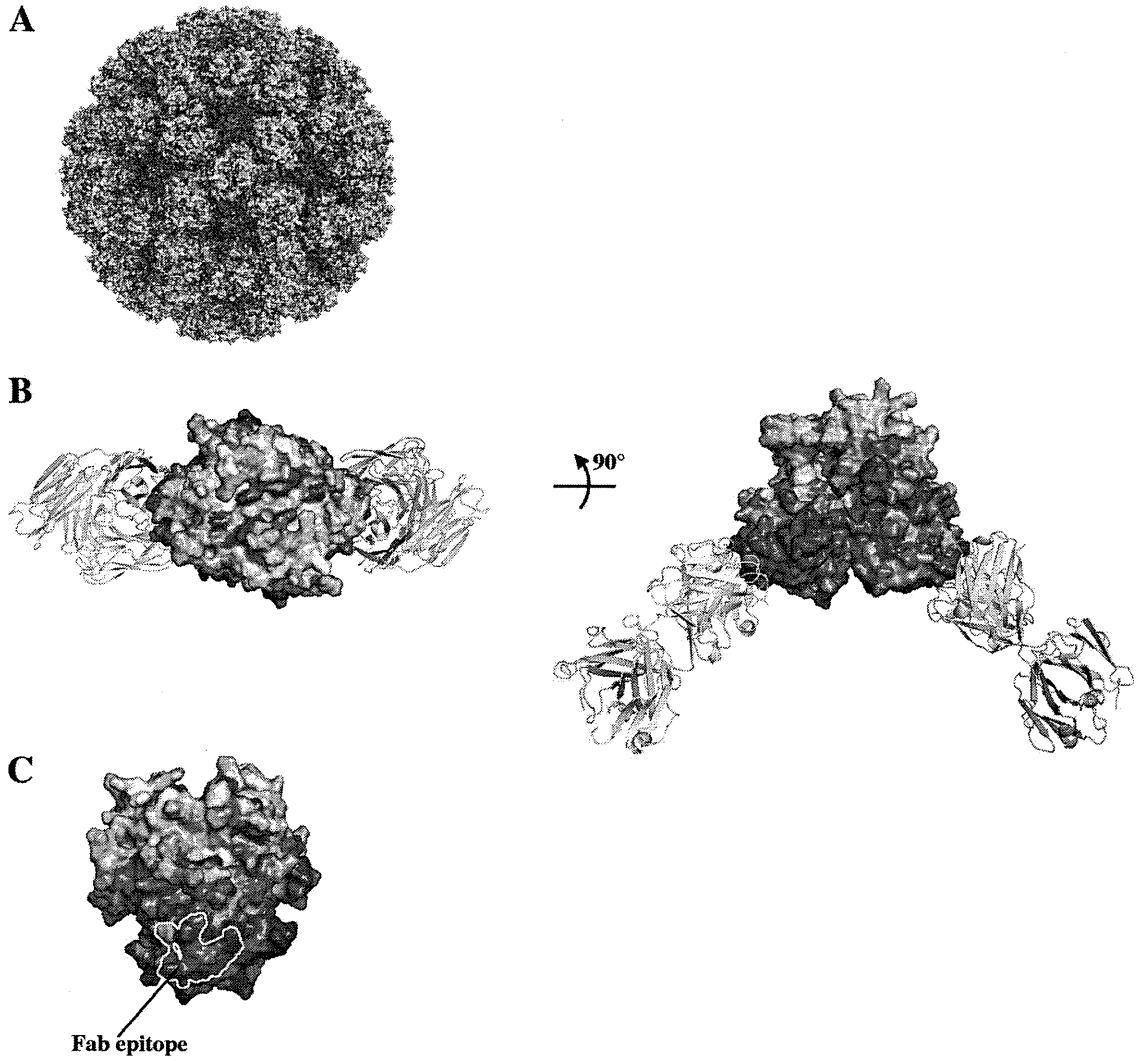


FIG 7 Surface representations of GII amino acid conservation. Noroviruses are genetically and antigenically distinct, with the S domain being more conserved than the P domain. (A) The GII amino acid variability was mapped onto the model of the GII.10 VLP (GI.1 S domain and GII.10 P domain). Amino acid conservation ranges are color-coded from deep purple (highly conserved) to white (highly variable). (B) The amino acid variability was mapped onto the GII.10 P domain apo structure (3ONU) with the 5B18 Fab bound. The top of the P domain was highly variable (left side), while the bottom half of the P domain was more conserved (right side). (C) The Fab binding footprint was mapped onto the P domain (yellow line). The footprint was at a highly conserved area on the wall of the P domain (inside the particle).

proximity to the 5B18 were all shown to detect VLPs (50, 59). These data therefore favor a model in which apparently intact norovirus capsids can indeed bind the 5B18 antibody (and other antibodies) despite significant steric clashes with the VLP structure.

Viruses often use remarkable conformational changes in their envelope or capsid structures to protect their genetic material by waiting for the proper cellular trigger to release their genome into the host cell. For example, the hemagglutinin spike in influenza undergoes a drastic pH-dependent conformational change in the endosome that initiates membrane fusion (8, 68). Similarly large pH-dependent changes have been observed with the enveloped flaviviruses (31, 32, 47) and alphaviruses (36, 45). Such changes due to environmental cues can expose or hide antigenic sites (e.g., see references 41, 45, and 47). Viruses can also receive cues via interactions with cellular receptors, as is the case with human rhinovirus (25, 26, 48). Viruses also undergo small, dynamic structural changes, "breathing" (6, 35, 37, 56), that are probably a prelude to the far larger conformational changes that occur during uncoating. These dynamic motions can transiently expose more-conserved antigenic sites that can be leveraged in designing vaccines (29, 37). However, the fact that these norovirus antibodies are recognizing deeply occluded portions of the P1 domain in apparently intact virions represents a different kind of viral dynamic: for this recognition to occur, the P domains must be capable of extremely large conformational changes without any obvious environmental cue. Such recognition would probably involve just one or a few P domains of a VLP being recognized by antibody 5B18; indeed, images of VLPs after incubation with an excess of antibody 5B18 for 1 h at 37°C (the same incubation used in the ELISA) shows them to be intact, with bound IgG difficult to detect (see Fig. S7 in the supplemental material).

Other antibodies have recently been described that bind to occluded sites on virions. With West Nile virus, the fusion loop-specific antibody E53 recognizes an epitope that should be inaccessible on mature virions. However, this antibody could neutralize mature West Nile virus in a time- and temperature-dependent manner, indicating a role of virus "breathing" or conformational dynamics in antibody recognition (17). With HIV-1, broadly neutralizing antibodies against the membrane-proximal external region of the virus do not appear to recognize the native viral spike (11, 58), again implicating conformational rearrangements to permit antibody recognition. These studies, along with the present study on norovirus recognition by 5B18, suggest substantial flexibility in certain virus particles as being important biologically for antibody-mediated recognition.

In summary, we have shown that a broadly reactive monoclonal antibody binds to an occluded site on the GII.10 P1 subdomain. The binding site was in close proximity to other monoclonal antibody binding sites, suggesting that the site contained an immunodominant region. We also found that the GII.10 VLP structure was more closely related to a GV.1 virion structure than to a GI.1 VLP structure and has marked flexibility in the P domains. These studies suggest that the P domain of noroviruses is capable of adopting variable conformations with respect to the S domain. Despite the vaunted diversity of noroviruses, especially on the exposed outer surface of the virion, one mechanism to achieve near pan-recognition by antibody may be to target a highly conserved domain interface that is dynamically exposed to the environment.

## ACKNOWLEDGMENTS

We thank J. Stuckey for assistance with figures and members of the Structural Biology Section at the NIH Vaccine Research Center for help with Fab preparation and comments on the manuscript, K. Nagayama for generous help and insightful discussions, and M. Kataoka for assistance with electron microscopy.

G.S.H. and P.D.K. conceived the project; G.S.H. performed X-ray crystallography and biochemical assays with assistance from J.S.M., S.-Y.P., and P.D.K.; D.W.T. determined the cryo-EM structure with assistance from K.M.; M.Y., F.G., M.M., and K.K. provided the 5B18 IgG; I.G. mapped sequence conservation onto the GII.10 VLP; and G.S.H., D.W.T., J.S.M., T.J.S., I.G., J.R.H.T., K.M., and P.D.K. analyzed the data and wrote the paper, on which all authors commented.

Support for this work was provided by the Intramural Research Program of the National Institutes of Health (NIAID [P.D.K.]), USA, and by a Grant-in-Aid for Scientific Research, grants from the Ministry of Health, Labor, and Welfare of Japan, and a grant from the National Institute of Natural Sciences (NINS), Japan (K.M.). D.W.T is an NSF Graduate Research Fellow and performed this work in Japan as a JSPS/NSF East Asia and Pacific Summer Institute Fellow. Use of Sector 22 (Southeast Region Collaborative Access team) at the Advanced Photon Source was supported by the U.S. Department of Energy, Basic Energy Sciences, Office of Science, under contract no. W-31-109-Eng-38.

## REFERENCES

1. **Adams PD, et al.** 2010. PHENIX: a comprehensive Python-based system for macromolecular structure solution. Acta Crystallogr. D. Biol. Crystallogr. **66**(Pt 2):213–221.
2. **Ausar SF, Foubert TR, Hudson MH, Vedvick TS, Middaugh CR.** 2006. Conformational stability and disassembly of Norwalk virus-like particles. Effect of pH and temperature. J. Biol. Chem. **281**:19478–19488.
3. **Belnap DM, et al.** 2000. Molecular tectonic model of virus structural transitions: the putative cell entry states of poliovirus. J. Virol. **74**:1342–1354.
4. **Bhella D, Gatherer D, Chaudhry Y, Pink R, Goodfellow IG.** 2008. Structural insights into calicivirus attachment and uncoating. J. Virol. **82**:8051–8058.
5. **Bhella D, Goodfellow IG.** 2011. The cryo-electron microscopy structure of feline calicivirus bound to junctional adhesion molecule A at 9-angstrom resolution reveals receptor-induced flexibility and two distinct conformational changes in the capsid protein VP1. J. Virol. **85**: 11381–11390.
6. **Bothner B, Dong XF, Bibbs L, Johnson JE, Siuzdak G.** 1998. Evidence of viral capsid dynamics using limited proteolysis and mass spectrometry. J. Biol. Chem. **273**:673–676.
7. **Bu W, et al.** 2008. Structural basis for the receptor binding specificity of Norwalk virus. J. Virol. **82**:5340–5347.
8. **Bullough PA, Hughson FM, Skehel JJ, Wiley DC.** 1994. Structure of influenza haemagglutinin at the pH of membrane fusion. Nature **371**: 37–43.
9. **Canady MA, Tihova M, Hanzlik TN, Johnson JE, Yeager M.** 2000. Large conformational changes in the maturation of a simple RNA virus, nudaurelia capensis omega virus (NomegaV). J. Mol. Biol. **299**:573–584.
10. **Cao S, et al.** 2007. Structural basis for the recognition of blood group trisaccharides by norovirus. J. Virol. **81**:5949–5957.
11. **Chakrabarti BK, et al.** 2011. Direct antibody access to the HIV-1 membrane-proximal external region positively correlates with neutralization sensitivity. J. Virol. **85**:8217–8226.
12. **Chen R, et al.** 2004. Inter- and intragenus structural variations in caliciviruses and their functional implications. J. Virol. **78**:6469–6479.
13. **Choi JM, Hutson AM, Estes MK, Prasad BV.** 2008. Atomic resolution structural characterization of recognition of histo-blood group antigens by Norwalk virus. Proc. Natl. Acad. Sci. U. S. A. **105**:9175–9180.
14. **Collaborative Computational Project N.** 1994. The CCP4 suite: programs for protein crystallography. Acta Crystallogr. D. Biol. Crystallogr. **50**:760–763.
15. **de Bruin E, Duizer E, Vennema H, Koopmans MP.** 2006. Diagnosis of Norovirus outbreaks by commercial ELISA or RT-PCR. J. Virol. Methods **137**:259–264.
16. **Dolinsky TJ, Nielsen JE, McCammon JA, Baker NA.** 2004. PDB2PQR: an automated pipeline for the setup of Poisson-Boltzmann electrostatics calculations. Nucleic Acids Res. **32**:W665–W667.
17. **Dowd KA, Jost CA, Durbin AP, Whitehead SS, Pierson TC.** 2011. A dynamic landscape for antibody binding modulates antibody-mediated neutralization of West Nile virus. PLoS Pathog. **7**:e1002111.
18. **Emsley P, Lohkamp B, Scott WG, Cowtan K.** 2010. Features and development of COOT. Acta Crystallogr. D. Biol. Crystallogr. **66**:486–501.
19. **Graham DY, et al.** 1994. Norwalk virus infection of volunteers: new insights based on improved assays. J. Infect. Dis. **170**:34–43.
20. **Greenberg HB, et al.** 1981. Proteins of Norwalk virus. J. Virol. **37**:994–999.
21. **Hansman GS, et al.** 2006. Genetic and antigenic diversity among noroviruses. J. Gen. Virol. **87**:909–919.
22. **Hansman GS, et al.** 2011. Crystal structures of GII.10 and GII.12 norovirus protruding domains in complex with histo-blood group antigens reveal details for a potential site of vulnerability. J. Virol. **85**:6687–6701.
23. **Hansman GS, et al.** 2004. Detection of norovirus and sapovirus infection among children with gastroenteritis in Ho Chi Minh City, Vietnam. Arch. Virol. **149**:1673–1688.
24. **Hardy ME, White LJ, Ball JM, Estes MK.** 1995. Specific proteolytic cleavage of recombinant Norwalk virus capsid protein. J. Virol. **69**:1693–1698.
25. **Hewat EA, Blaas D.** 2004. Cryoelectron microscopy analysis of the structural changes associated with human rhinovirus type 14 uncoating. J. Virol. **78**:2935–2942.
26. **Hoover-Litty H, Greve JM.** 1993. Formation of rhinovirus-soluble ICAM-1 complexes and conformational changes in the virion. J. Virol. **67**:390–397.
27. **Jiang X, Wang M, Graham DY, Estes MK.** 1992. Expression, self-assembly, and antigenicity of the Norwalk virus capsid protein. J. Virol. **66**:6527–6532.
28. **Kamata K, et al.** 2005. Expression and antigenicity of virus-like particles of norovirus and their application for detection of noroviruses in stool samples. J. Med. Virol. **76**:129–136.
29. **Katpally U, Fu T, Freed DC, Casimiro DR, Smith TJ.** 2009. Antibodies to the buried N-terminus of rhinovirus VP4 exhibit cross-serotypic neutralization. J. Virol. **83**:7040–7048.

30. **Katpally U, et al.** 2010. High-resolution cryo-electron microscopy structures of murine norovirus 1 and rabbit hemorrhagic disease virus reveal marked flexibility in the receptor binding domains. J. Virol. **84**:5836–5841.
31. **Kaufmann B, et al.** 2009. Capturing a flavivirus pre-fusion intermediate. PLoS Pathog. **5**:e1000672.
32. **Kaufmann B, et al.** 2006. West Nile virus in complex with the Fab fragment of a neutralizing monoclonal antibody. Proc. Natl. Acad. Sci. U. S. A. **103**:12400–12404.
33. **Krissinel E, Henrick K.** 2007. Inference of macromolecular assemblies from crystalline state. J. Mol. Biol. **372**:774–797.
34. **Kwong PD, et al.** 1999. Probability analysis of variational crystallization and its application to gp120, the exterior envelope glycoprotein of type 1 human immunodeficiency virus (HIV-1). J. Biol. Chem. **274**:4115–4123.
35. **Lewis JK, Bothner B, Smith TJ, Siuzdak G.** 1998. Antiviral agent blocks breathing of the common cold virus. Proc. Natl. Acad. Sci. U. S. A. **95**:6774–6778.
36. **Li L, Jose J, Xiang Y, Kuhn RJ, Rossmann MG.** 2010. Structural changes of envelope proteins during alphavirus fusion. Nature **468**:705–708.
37. **Li Q, Yafal AG, Lee YMH, Hogle J, Chow M.** 1994. Poliovirus neutralization by antibodies to internal epitopes of VP4 and VP1 results from reversible exposure of the sequences at physiological temperatures. J. Virol. **68**:3965–3970.
38. **Li TC, et al.** 2005. Essential elements of the capsid protein for self-assembly into empty virus-like particles of hepatitis E virus. J. Virol. **79**:12999–13006.
39. **Li X, Zhou R, Tian X, Li H, Zhou Z.** 2010. Characterization of a cross-reactive monoclonal antibody against Norovirus genogroups I, II, III and V. Virus Res. **151**:142–147.
40. **Lochridge VP, Jutila KL, Graff JW, Hardy ME.** 2005. Epitopes in the P2 domain of norovirus VP1 recognized by monoclonal antibodies that block cell interactions. J. Gen. Virol. **86**:2799–2806.
41. **Lok S-M, et al.** 2008. Binding of a neutralizing antibody to dengue virus alters the arrangement of surface glycoproteins. Nat. Struct. Mol. Biol. **15**:312–317.
42. **Majeed S, et al.** 2003. Enhancing protein crystallization through precipitant synergy. Structure **11**:1061–1070.
43. **Matsui T, Lander G, Johnson JE.** 2009. Characterization of large conformational changes and autoproteolysis in the maturation of a T=4 virus capsid. J. Virol. **83**:1126–1134.
44. **McCoy AJ, et al.** 2007. Phaser crystallographic software. J. Appl. Crystallogr. **40**:658–674.
45. **Meyer WJ, Gidwitz S, Ayers VK, Schoepp RJ, Johnston RE.** 1992. Conformational alteration of Sindbis virion glycoproteins induced by heat, reducing agents, or low pH. J. Virol. **66**:3504–3513.
46. **Miao Y, Johnson JE, Ortoleva PJ.** 2010. All-atom multiscale simulation of cowpea chlorotic mottle virus capsid swelling. J. Phys. Chem. B. **114**:11181–11195.
47. **Modis Y, Ogata S, Clements D, Harrison SC.** 2004. Structure of the dengue virus envelope protein after membrane fusion. Nature **427**:313–319.
48. **Olson NH, et al.** 1993. Structure of a human rhinovirus complexed with its receptor molecule. Proc. Natl. Acad. Sci. U. S. A. **90**:507–511.
49. **Otwinowski Z, Minor W.** 1997. Processing of X-ray diffraction data collected in oscillation mode. Methods Enzymol. **276**:307–326.
50. **Parker TD, Kitamoto N, Tanaka T, Hutson AM, Estes MK.** 2005. Identification of genogroup I and genogroup II broadly reactive epitopes on the norovirus capsid. J. Virol. **79**:7402–7409.
51. **Pei J, Grishin NV.** 2001. AL2CO: calculation of positional conservation in a protein sequence alignment. Bioinformatics **17**:700–712.
52. **Pettersen EF, et al.** 2004. UCSF Chimera—a visualization system for exploratory research and analysis. J. Comput. Chem. **25**:1605–1612.
53. **Prasad BV, et al.** 1999. X-ray crystallographic structure of the Norwalk virus capsid. Science **286**:287–290.
54. **Prasad BV, Rothnagel R, Jiang X, Estes MK.** 1994. Three-dimensional structure of baculovirus-expressed Norwalk virus capsids. J. Virol. **68**:5117–5125.
55. **Rabenau HF, et al.** 2003. Laboratory diagnosis of norovirus: which method is the best? Intervirology **46**:232–238.
56. **Reisdorph N, et al.** 2003. Human rhinovirus capsid dynamics is controlled by canyon flexibility. Virology **314**:34–44.
57. **Richards AF, et al.** 2003. Evaluation of a commercial ELISA for detecting Norwalk-like virus antigen in faeces. J. Clin. Virol. **26**:109–115.
58. **Ruprecht CR, et al.** 2011. MPER-specific antibodies induce gp120 shedding and irreversibly neutralize HIV-1. J. Exp. Med. **208**:439–454.
59. **Shiota T, et al.** 2007. Characterization of a broadly reactive monoclonal antibody against norovirus genogroups I and II: recognition of a novel conformational epitope. J. Virol. **81**:12298–12306.
60. **Tan M, Hegde RS, Jiang X.** 2004. The P domain of norovirus capsid protein forms dimer and binds to histo-blood group antigen receptors. J. Virol. **78**:6233–6242.
61. **Tang G, et al.** 2007. EMAN2: an extensible image processing suite for electron microscopy. J. Struct. Biol. **157**:38–46.
62. **Tang J, et al.** 2009. Dynamics and stability in maturation of a T=4 virus. J. Mol. Biol. **392**:803–812.
63. **Taube S, et al.** 2010. High-resolution X-ray structure and functional analysis of the murine norovirus 1 capsid protein protruding domain. J. Virol. **84**:5695–5705.
64. **Trus BL, et al.** 1996. The herpes simplex virus procapsid: structure, conformational changes upon maturation, and roles of the triplex proteins VP19c and VP23 in assembly. J. Mol. Biol. **263**:447–462.
65. **van Heel M, Harauz G, Orlova EV, Schmidt R, Schatz M.** 1996. A new generation of the IMAGIC image processing system. J. Struct. Biol. **116**:17–24.
66. **Ward VK, et al.** 2007. Recovery of infectious murine norovirus using pol II-driven expression of full-length cDNA. Proc. Natl. Acad. Sci. U. S. A. **104**:11050–11055.
67. **Widdowson M-A, et al.** 2005. Detection of serum antibodies to bovine norovirus in veterinarians and the general population in the Netherlands. J. Med. Virol. **76**:119–128.
68. **Wilson IA, Skehel JJ, Wiley DC.** 1981. Structure of the haemagglutinin membrane glycoprotein of influenza virus at 3Å resolution. Nature **289**:366–373.
69. **Wobus CE, Thackray LB, Virgin HW.** 2006. Murine norovirus: a model system to study norovirus biology and pathogenesis. J. Virol. **80**:5104–5112.
70. **Yoda T, et al.** 2003. Precise characterization of norovirus (Norwalk-like virus)-specific monoclonal antibodies with broad reactivity. J. Clin. Microbiol. **41**:2367–2371.
71. **Yu IM, et al.** 2008. Structure of the immature dengue virus at low pH primes proteolytic maturation. Science **319**:1834–1837.
72. **Zheng DP, et al.** 2006. Norovirus classification and proposed strain nomenclature. Virology **346**:312–323.

Journal of Virology

# Structural Basis for Norovirus Inhibition and Fucose Mimicry by Citrate

**Grant S. Hansman, Syed Shahzad-ul-Hussan, Jason S. McLellan, Gwo-Yu Chuang, Ivelin Georgiev, Takashi Shimoike, Kazuhiko Katayama, Carole A. Bewley and Peter D. Kwong**

*J. Virol.* 2012, 86(1):284. DOI: 10.1128/JVI.05909-11.
Published Ahead of Print 26 October 2011.

JVI Journals.ASM.org

# Structural Basis for Norovirus Inhibition and Fucose Mimicry by Citrate

**Grant S. Hansman,[a,b] Syed Shahzad-ul-Hussan,[a,c] Jason S. McLellan,[a] Gwo-Yu Chuang,[a] Ivelin Georgiev,[a] Takashi Shimoike,[b] Kazuhiko Katayama,[b] Carole A. Bewley,[c] and Peter D. Kwong[a]**

Vaccine Research Center, National Institute of Allergy and Infectious Diseases, National Institutes of Health, Bethesda, Maryland 20892, USA[a]; Department of Virology II, National Institute of Infectious Diseases, Tokyo, 208-0011, Japan[b]; and Laboratory of Bioorganic Chemistry, National Institute of Diabetes and Digestive and Kidney Diseases, National Institutes of Health, Bethesda, Maryland 20892, USA[c]

**Human noroviruses bind with their capsid-protruding domains to histo-blood-group antigens (HBGAs), an interaction thought to direct their entry into cells. Although human noroviruses are the major cause of gastroenteritis outbreaks, development of antivirals has been lacking, mainly because human noroviruses cannot be cultivated. Here we use X-ray crystallography and saturation transfer difference nuclear magnetic resonance (STD NMR) to analyze the interaction of citrate with genogroup II (GII) noroviruses. Crystals of citrate in complex with the protruding domain from norovirus GII.10 Vietnam026 diffracted to 1.4 Å and showed a single citrate bound at the site of HBGA interaction. The citrate interaction was coordinated with a set of capsid interactions almost identical to that involved in recognizing the terminal HBGA fucose, the saccharide which forms the primary conserved interaction between HBGAs and GII noroviruses. Citrate and a water molecule formed a ring-like structure that mimicked the pyranoside ring of fucose. STD NMR showed the protruding domain to have weak affinity for citrate (460 $\mu$M). This affinity, however, was similar to the affinities of the protruding domain for fucose (460 $\mu$M) and H type 2 trisaccharide (390 $\mu$M), an HBGA shown previously to be specifically recognized by human noroviruses. Importantly, competition STD NMR showed that citrate could compete with HBGA for norovirus binding. Together, the results suggest that citrate and other glycomimetics have the potential to block human noroviruses from binding to HBGAs.**

Human noroviruses, family *Caliciviridae*, are the dominant cause of outbreaks of gastroenteritis. Many aspects of human norovirus replication, however, remain unclear, mainly because these viruses cannot be grown in cell culture. Transmission predominately occurs through ingestion of contaminated foods, airborne transmission, and person-to-person contact. Medical treatment usually involves orally administered fluids and electrolyte replacement therapy. Currently, there is no effective vaccine.

Human noroviruses can be divided into 2 main genogroups (GI and GII), which can be further subdivided into at least 25 different genotypes (GI.1 to -8 and GII.1 to -17) (26, 57). The norovirus genome has three open reading frames (ORFs) that encode nonstructural, capsid, and small structural proteins, respectively. The capsid of human norovirus is composed of two domains, shell and protruding (P) domains. The shell forms a scaffold around the RNA, and the dimeric P domain contains determinants for both antigenicity and receptor binding (25, 43, 51). The P domain is further subdivided into P1 and P2 subdomains, where the P1 subdomain interacts with the shell domain and is buried under the outermost P2 subdomain.

Human noroviruses bind to histo-blood group antigens (HBGAs), with recognition occurring in the P domain. HBGAs are complex carbohydrates present on mucosal epithelial cells or free antigens in blood, saliva, and other fluids (32). X-ray crystal structures of norovirus P domains in complex with different HBGAs have defined distinct binding sites for GI and GII viruses (8, 11, 12, 21); in particular, the HBGA binding site of GII is located at the dimeric interface of two P domains, whereas the HBGA binding site in GI is located within a single P domain (8, 11, 12, 21).

A number of recent studies have shown that natural fruits or their constituents, including orange juice, pomegranate juice, cranberry juice, and grape seed extract, can inhibit and/or reduce feline calicivirus and murine norovirus infectivity (23, 48–50, 54). Although there have been no studies to support the idea that natural fruits or their constituents can prevent human norovirus infections, and data on the mode of inhibition of fruits have been lacking, the stability of human norovirus virus-like particles over a pH range of 3 to 7 (3) suggested that the effect might be related to a specific interaction with compounds in fruits rather than a pH effect. In this study, we used X-ray crystallography and saturation transfer difference nuclear magnetic resonance (STD NMR) to provide atomic-level details on the interaction of citrate and GII human noroviruses. We show that citrate specifically binds at the HBGA recognition site of GII noroviruses, and this inhibits P domain binding of both fucose and HBGA.

## MATERIALS AND METHODS

**Protein expression, purification, and crystallization of the norovirus P domain.** The norovirus Vietnam026 GII.10 P domain (GenBank accession no. AF504671) (22) was expressed in *Escherichia coli* as previously

**Received** 5 August 2011 **Accepted** 17 October 2011
**Published ahead of print** 26 October 2011
Address correspondence to Peter D. Kwong, pkwong@mail.nih.gov, or Carole A. Bewley, caroleb@mail.nih.gov.
G.S.H. and S.S.H. contributed equally to this article.
Supplemental material for this article may be found at http://jvi.asm.org/.

doi:10.1128/JVI.05909-11

described (21). Briefly, a truncated form of the GII.10 P domain was optimized for *E. coli* expression, cloned in a modified pMal-c2x vector at the BamHI and NotI sites (New England BioLabs), and transformed into *E. coli* BL21 cells (Invitrogen), and expression was induced with 1 mM IPTG (isopropyl-β-D-thiogalactopyranoside) for 18 h at 22°C. After a series of purifications and cleavage steps, the P domain was concentrated to 2 mg/ml and stored in gel filtration buffer (0.35 M NaCl, 2.5 mM Tris [pH 7.0], 0.02% $NaN_3$) before crystallization. Crystals of the P domain were obtained by the hanging-drop vapor diffusion method, with the mother solution containing citric acid triammonium (0.66 M [pH 6.5]) and isopropanol (1.65% [vol/vol]).

**Data collection, structure solution, and refinement.** X-ray diffraction data at a 1.000-Å wavelength were collected at the Southeast Regional Collaborative Access Team (SER-CAT) beamline 22-BM at the Advanced Photon Source, Argonne National Laboratory, Argonne, IL, and processed with HKL2000 (41). Prior to data collection, crystals were transferred to a cryoprotectant solution consisting of the mother liquor in 30% ethylene glycol, loop mounted, and flash-cooled in a nitrogen cryostat to 100°K. Structures were solved by molecular replacement with PHASER (35) by using Protein Data Bank (PDB) code 2OBR (11) as a search model. Structures were refined in multiple rounds of manual model building in COOT (16) and positional together with TLS refinement in REFMAC (13) and PHENIX (1).

**Structure analysis and figures.** Citrate and H type 2 interactions were determined using Discovery Studio (Accelrys, version v2.5.5.9350). Figures were rendered using PyMOL (Schroedinger, LLC, version 1.2r3) and ChemDraw Ultra (Cambridgesoft, version 12.0.2.1076).

**STD NMR.** All NMR data were recorded at 298°K on a Bruker Avance 600 NMR spectrometer equipped with a cryogenically cooled *z*-shielded gradient probe. One-dimensional (1D) STD NMR spectra were acquired with selective irradiation at −1 and +40 ppm (on and off resonance, respectively) using a train of 50-ms Gaussian-shaped radio frequency pulses separated by 1-ms delays and an optimized power level of 57 db. Water suppression was achieved with a binomial 3-9-19 pulse sequence. Samples were prepared in 20 mM sodium phosphate buffer containing 50 mM sodium chloride at pH 6.8. The NMR data were processed and analyzed with Topspin 2.1. STD enhancements were expressed as the STD amplification factor, $A_{STD}$, defined as $A_{STD} = (I_0 - I_{SAT})\, I_0^{-1}\, ([L_t]/[P])$, where $L_t$ and $P$ are the total ligand and protein concentrations, respectively (34). HBGAs, H type 2 disaccharide [α-L-fucose-(1-2)-β-D-galactose], and H type 2 trisaccharide [α-L-fucose-(1-2)-β-D-galactose-(1-4)-2-*N*-acetyl-β-D-glucosamine] were purchased from V-labs, and L-fucose was purchased from Sigma-Aldrich. For the citrate experiments, sodium citrate dihydrate (Sigma-Aldrich) was added to sodium phosphate buffer and then titrated at pH 6.85 ± 0.1.

**Computational citrate docking studies of other saccharide-binding proteins.** Citrate docking analyses were performed against six different saccharide-binding proteins, including *Anguilla anguilla* agglutinin (PDB identification no. 1K12) (5), *Aleuria aurantia* lectin (PDB identification no. 1IUC) (19), *Streptococcus pneumoniae* virulence factor SpGH98 (PDB identification no. 2J1S) (7), *Pseudomonas aeruginosa* PA-IIL lectin (PDB identification no. 2JDH) (33), parainfluenza virus 5 hemagglutinin-neuraminidase (PDB identification no. 1Z4X) (56), and porcine adenovirus type 4 galectin domain (PDB identification no. 2WSV) (20). Water molecules and ligands were removed from the PDB files, with the exception of one water molecule (HOH 935) in 1Z4X, which is present in both ligand-free and sialyllactose-bound hemagglutinin-neuraminidase structures. For 2JDH, the two calcium ions in the fucose binding site were kept, and the partial charges for the calcium ions were assigned to 1.5 as suggested by previous studies (38). AutoDock4.2 (39) was used as the docking engine, with the grid files generated by Autogrid4.2 using default parameters and centered on the cocrystallized ligands. The citrate molecule was docked to the three structures using default parameters (ga_pop_size = 150, ga_num_evals = 2,500,000, and ga_run = 50). For each structure, the docking pose with the lowest estimated free energy of binding among the 50 docking runs was selected as the predicted binding pose. For comparison, for each complex, the cocrystallized ligand (or the terminal monosaccharide having the largest contact area with the binding site, if the cocrystallized ligand was not a monosaccharide) was docked in the saccharide binding site using the same procedure. Fucose and citrate molecules were also docked to the fucose-bound GII.10 P domain (PDB identification no. 3ONY) and the citrate-bound GII.10 P domain, respectively, for comparison. The water molecule (HOH 135) mediating the interaction between citrate and the protein was present during the citrate docking analysis.

**Protein structure accession number.** Atomic coordinate and structure factors for the citrate-bound GII.10 P domain have been deposited in the Protein Data Bank under accession no. 3RY8.

## RESULTS

**X-ray crystal structure of citrate bound to the GII.10 P domain.** The GII.10 P domain protein could be expressed in *E. coli* to 2 mg/liter and was purified and prepared for crystallization as previously described (21). To obtain a GII.10 P domain-citrate complex, we chose a crystallization condition that was similar to our previously reported GII.10 P domain-HBGA complex conditions (21), though with the addition of citrate. The GII.10 P domain-citrate complex formed rectangular plate crystals, and X-ray diffraction data revealed a space group of $P2_1$, the same as the previous GII.10 P domain-HBGA complexes (21), and strong diffraction to 1.4 Å. Structure solution by molecular replacement revealed one dimer per asymmetrical unit (Fig. 1A), and refinement led to an $R_{value}$ of 0.139 ($R_{free}$ = 0.151), with well-defined density for most of the P domain dimer (Table 1). Electron density for residues 296 to 299 (chain A) and 296 to 300 and 344 to 351 (chain B) was poor, and these residues were not modeled. Extra electron density was observed at the HBGA binding site, where a single citrate molecule was clearly distinguished and refined (Fig. 1B; see Fig. S1 in the supplemental material). The structure of the GII.10 P domain in complex with citrate was highly reminiscent of the other known structures (GI.1, GII.4, and GII.12), where the P1 subdomain contains a single α-helix and the P2 subdomain contains six anti-parallel β-strands that form two anti-parallel β-sheets (21).

**Citrate was highly coordinated by the GII.10 P domain.** At a 1.4-Å resolution, detailed interactions between citrate and the P domain could be defined. Seven residues of the P domain, many of which are conserved and located at the dimer interface, are involved in hydrogen bonding interactions with citrate (Fig. 1B and C). These include the side chain of Tyr452 and main chain of Gly451 from one P domain subunit as well as side chains Arg356 and Asp385 and the main chain of Asn355 of a second P domain subunit. Unique to citrate binding, side chains of Asn342 and Ser387 make a water-mediated hydrogen bond with the C-5 CO group of citrate. Superposition of citrate-bound and apo GII.10 P domain structures indicated that the citrate interaction did not cause any conformation changes in the GII.10 P domain.

**Comparisons of citrate and HBGA interaction with the GII.10 P domain.** Compared with GII.10 P domains in complex with HBGAs, we found that citrate essentially mimics the fucose unit of HBGAs. By using H type 2 di- and trisaccharides as examples, superposition of the P domains revealed that three carbon atoms, including C-2, C-3, and the C-3 carboxy carbon, and three oxygen atoms, including the C-1 and C-3 carboxy oxygens and the C-3 hydroxyl group of citrate closely overlapped with C-5/C-4/C-3/O-5/O-4/O-3 of the terminal α-fucose ring (Fig. 2). In addition,

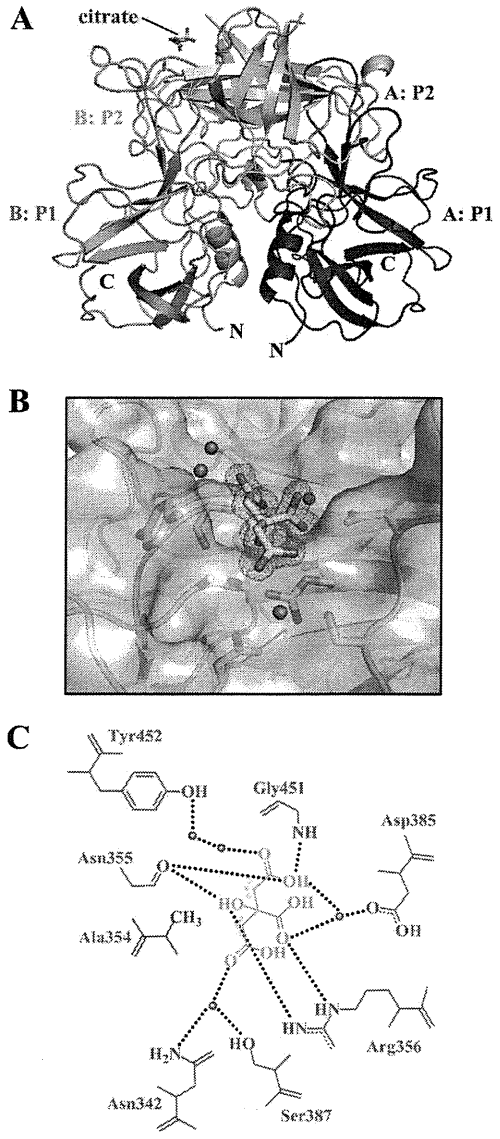


FIG 1 Citrate binding to the GII.10 P domain. (A) X-ray crystal structure of the GII.10 P domain dimer (ribbon structure) and the bound citrate (green sticks). Each P subdomain is colored differently: i.e., chain A, P1, blue; chain A, P2, light blue; chain B, P1, violet; and chain B, P2, salmon. (B) Surface representation of the GII.10 P domain (colored as in panel A) showing the residues (sticks) and water molecules (red spheres) interacting with the citrate molecule (green sticks). The $2F_o$-$F_c$ density was contoured at 1.0 $\sigma$. (C) Residues interacting with the citrate molecule were contributed by both monomers (colored as in panel A), where the black dotted lines represent the hydrogen bonds, the cyan dots near the citrate represent the hydrophobic interactions with Ala354, and the red spheres represent water molecules. For simplicity, only the backbone is shown for residues that were backbone mediated. Hydrogen bond distances were less than 3.1 Å, though the majority were ~2.8 Å.

a water molecule, present in the citrate-bound structure but absent from the HBGA-bound structures, occupied the site of the C-2 hydroxyl of fucose (Fig. 2). In this configuration, the citrate and associated water molecule formed a ring-like structure, mimicking the pyranoside ring of fucose. Finally, the comparisons showed that of the seven residues involved in hydrogen bonding interactions with citrate, five made almost identical interactions with their comparable atoms in fucose.

**Characterization of binding of citrate, H type 2 trisaccharide, and fucose to GII.10 P domain by STD NMR.** Given the remarkable similarities observed for citrate and fucose binding to the GII.10 P domain by crystallography, we sought to characterize in solution by NMR the binding of GII.10 P domain with citrate, HBGAs, and fucose and ultimately to determine their relative binding affinities and whether they bind competitively.

STD enhancements were observed for methylene protons H2A and H2B of citrate, consistent with their close proximity to the protein in the bound state (Fig. 3A). In the crystal structure, these hydrogens are within van der Waals contact of the methyl of Ala354 (Fig. 1C). With H type 2 trisaccharide, the most prominent STD signals that could be assigned corresponded to H-1, H-2, and H-4 of $\alpha$-fucose; H-3 of galactose; and H-1, H-2, and *N*-acetyl of glucosamine (Fig. 3B). We also characterized binding of monosaccharide $\alpha/\beta$-fucopyranose, as it also would be used in competition STD NMR experiments. As seen in Fig. 3C, binding of both anomers was observed, with H-1, H-2, and H-4 of $\alpha$-fucose versus H-2, H-4, and H-5 of $\beta$-fucose showing the strongest enhancements. Although natural H type 2 HBGAs contain $\alpha$-Fuc(1-2)Gal and not $\beta$-Fuc, it is interesting that the HBGA binding site of norovirus can bind both. By NMR, we observed binding of $\alpha$ and $\beta$ forms of the monosaccharide (Fig. 3C) as well as synthetic H type 2 trisaccharide $\alpha/\beta$-Fuc(1-2)$\beta$-Gal(1-4)$\beta$-GlcN (Fig. 3B) and H type 2 disaccharide $\alpha$-Fuc(1-2)$\beta$-Gal(1-4) (data not shown), and by crystallography, binding of synthetic H type 2

TABLE 1 Data collection and refinement statistics for structures of the GII.10 Vietnam026 norovirus P domain[a]

| Parameter | Value(s) for citrate (026_citrate; PDB accession no. 3RY8)[b] |
|---|---|
| Data collection | |
| Space group | $P2_1$ |
| Cell dimensions | |
| *a*, *b*, *c* (Å) | 63.76, 79.81, 69.60 |
| $\alpha$, $\beta$, $\gamma$ (°) | 90, 96.84, 90 |
| Resolution (Å) | 50-1.40 (1.45-1.40) |
| $R_{sym}$ | 7.3 (30.5) |
| $I/\sigma I$ | 18.7 (3.2) |
| Completeness (%) | 99.9 (99.6) |
| Redundancy | 3.7 (3.2) |
| Refinement | |
| Resolution range (Å) | 31.98-1.399 |
| No. of reflections | 131,576 |
| $R_{work}/R_{free}$ | 0.1388/0.1506 |
| No. of atoms: | |
| Total | 5,587 |
| Protein | 4,722 |
| Ligand/ion | 57 |
| Water | 808 |
| *B*-factors | |
| Protein | 18.3 |
| Ligand/ion | 19.2 |
| Water | 30.2 |
| RMSD | |
| Bond length (Å) | 0.011 |
| Bond angle (°) | 1.393 |

[a] Each data set was collected from a single crystal.
[b] Values in parentheses are for the highest-resolution shell.

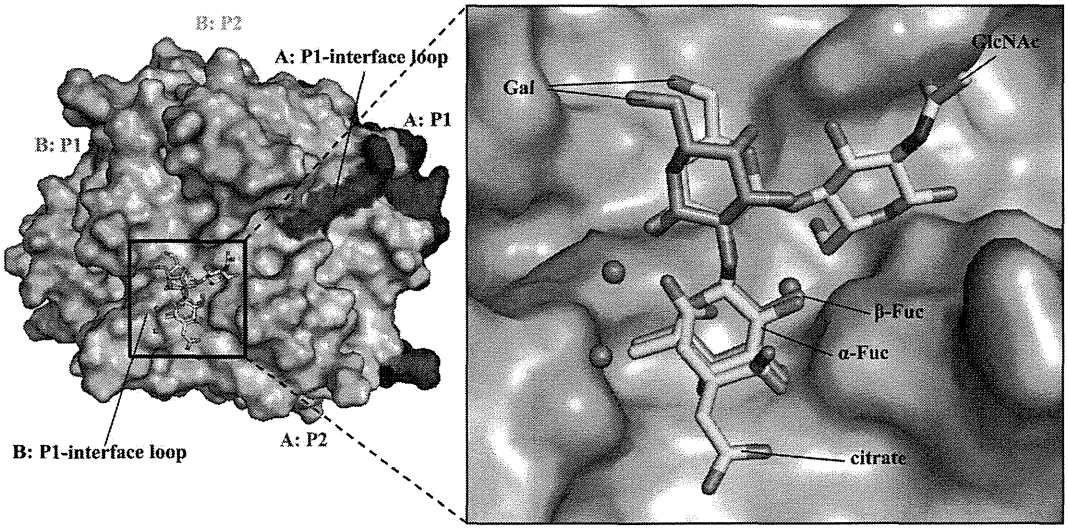


FIG 2 The HBGA and citrate binding site overlapped on the top of the GII.10 P domain. (A) The citrate molecule (green sticks) bound at the HBGA binding site; shown here are the bound H type 2 di- and trisaccharides (orange and cyan sticks, respectively). (B) Close-up of the black square in panel A, showing the H type 2 disaccharide [α-L-fucose(1-2)-β-D-galactose] and H type 2 trisaccharide [β-L-fucose(1-2)-β-D-galactose(1-4)-2-*N*-acetyl-β-D-glucosamine].

trisaccharide β-Fuc(1-2)β-Gal(1-4)β-GlcN was observed, in addition to binding of other HBGAs containing the α-Fuc(1-2)β-Gal linkage (21). Finally, it is interesting to note that a similar mode of citrate binding was observed for the soluble GII.12 P domain (see Fig. S2 in the supplemental material).

**Affinity of citrate, H type 2 tri- and disaccharides, and L-fucose to the GII.10 P domain.** We used single-ligand titration STD NMR experiments to determine the $K_D$ (equilibrium dissociation constant) of citrate binding to the GII.10 P domain (Fig. 4A) (2). STD amplification factors ($A_{STD}$) (34) were calculated by integrating the signal at $\delta_H$ 2.54 ppm in difference and corresponding reference spectra. Initial growth rates ($A_{0STD}$) were obtained by measuring the effect on $A_{STD}$ as a function of various saturation time ($t_{sat}$) and fitting the data to the equation $A_{STD} = A_{max\ STD}[1 - \exp(-kt_{sat})]$ for each concentration (300, 600, 900, 1,200, and 1,500 μM) of the ligand. The $K_D$ of citrate was in turn measured as 460 ± 80 μM by fitting $A_{0STD}$ values as a function of ligand concentration using the equation $y = B_{max}/(K_D + x)$, where $x$ is the ligand concentration and $B_{max}$ represents the plateau of the curve (Fig. 4) (2, 37). For H type 2 trisaccharide, the STD enhancements for the *N*-acetyl signal were sufficiently strong to allow for accurate integration, even at very short saturation times (0.1 s); thus, a $K_D$ value of 390 ± 70 μM could be determined directly by fitting $A_{STD}$ values as a function of ligand concentration (40) (Fig. 5). $K_D$ values for fucose and H type 2 disaccharides were in turn obtained from single point competition STD experiments as described previously (36) to give values of 460 ± 10 and 420 ± 40 μM, respectively (see Fig. S3 in the supplemental material).

**Competition of HBGAs and citrate with the GII.10 P domain.** To confirm the overlapping mode of binding observed in the crystal structure of citrate and fucose of H type 2 ligands, $A_{STD}$ values of L-fucopyranose and H type 2 trisaccharide were monitored while titrating citrate to the samples. As seen in Fig. 4E, addition of citrate to a sample of P domain-H type 2 trisaccharide diminishes the trisaccharide signals in a concentration-dependent manner, indicating that citrate directly competes with the trisaccharide for P domain binding, giving a $K_i$ of 600 ± 20 μM. Upon addition of citrate, the pH of the solutions was found to remain constant (pH 7.2 ± 0.1), indicating that the competition was a direct result of citrate binding rather than pH. The same effect was observed in STD competition experiments with L-fucose (data not shown). Importantly, the reverse set of experiments showed that HBGAs can compete with citrate for P domain binding (data not shown), indicating that the P domain is unaffected by the presence of citrate. Together, these results conclusively demonstrate molecular mimicry between citrate and fucose of HBGAs.

## DISCUSSION

Despite the discovery of human norovirus nearly 40 years ago (27), little is known about the capsid interaction with ligands (18, 44) other than HBGAs (8, 11, 12, 15, 21, 45). Our finding that citrate binds at the terminal fucose binding site was somewhat unexpected, given that the structure of citrate is unlike the structure of fucose and considering that the GII.10 P domain could not bind HBGAs having an α-fucose1-3/4 saccharide (21). In an earlier enzyme immune assay study, Feng et al. screened ~5,000 compounds (the Diversity screening set; Timtec, Inc.) for their ability to block GI and GII norovirus virus-like particles (VLPs) from binding to saliva samples of known HBGA type (18). They found 14 compounds that had strong inhibition; however, the mode of action was not determined. In a more recent NMR study, Rademacher et al. screened ~500 compounds (the Maybridge Ro5 fragment library; Thermo Fisher Scientific, Inc.) for their ability to bind to a GII.4 VLP HBGA binding site (44). They showed that both univalent and multivalent compounds were capable of binding to the HBGA binding site. Interestingly, for both studies, the compounds that showed the highest affinities included compounds with at least one ring component. Taken together, these studies indicated that the HBGA binding site was capable of binding numerous compounds other than HBGAs, ranging from the small (smallest) citrate molecule to larger multivalent compounds.

For over a decade, the GII.4 noroviruses have remained as the dominant genotype of outbreaks of gastroenteritis around the

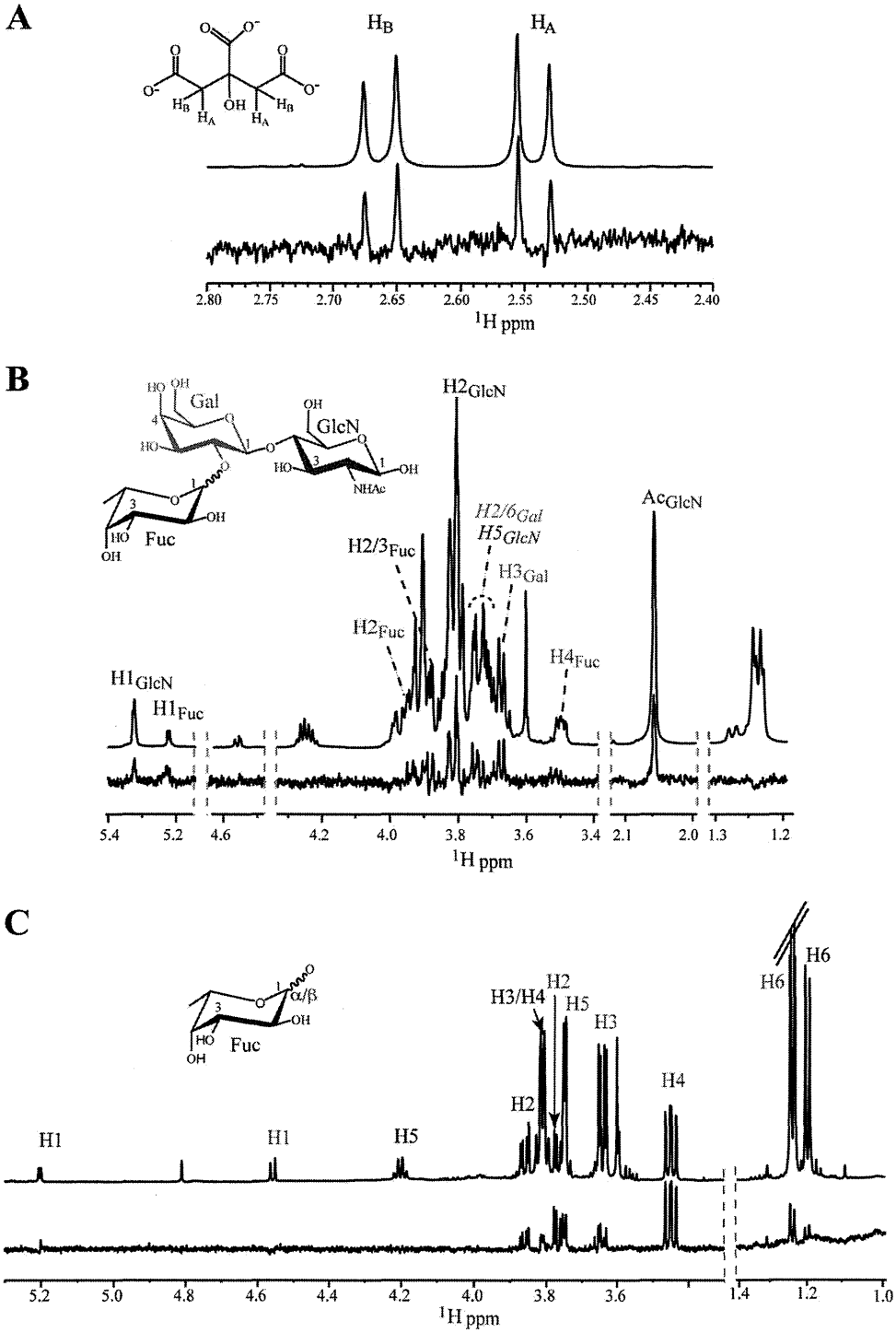


FIG 3 STD NMR spectra for citrate, H type 2 trisaccharide, and L-fucose bound to the GII.10 P domain. STD (lower) and reference (upper) spectra of (A) citrate (1.2 mM), (B) H type 2 trisaccharide (1.2 mM), and (C) L-fucose (mixture of $\alpha$ and $\beta$ anomers) (1.2 mM) in the presence of the GII.10 P domain (15 $\mu$M). Nonoverlapping protons that exhibit STD enhancements are labeled and color coded by sugar residue, and signals for $\beta$-Fuc are red. One group of overlapping signals appears in italics.

world and as such the most well studied. Most studies agreed that a dominant GII.4 norovirus was replaced the following year or next by a new GII.4 "variant" norovirus that had ~5% amino acid change in the capsid gene (6, 9, 10, 30, 31, 47). The reason that the GII.4 variants dominated and not some other genotype was unknown, but studies have shown specific mutations at or surrounding the HBGA binding site were capable of altering the HBGA binding patterns (15, 30, 31, 52). These small changes were thought to lead to new GII.4 variants capable of causing pandemics, analogous to influenza A virus evolution (14, 29). Despite

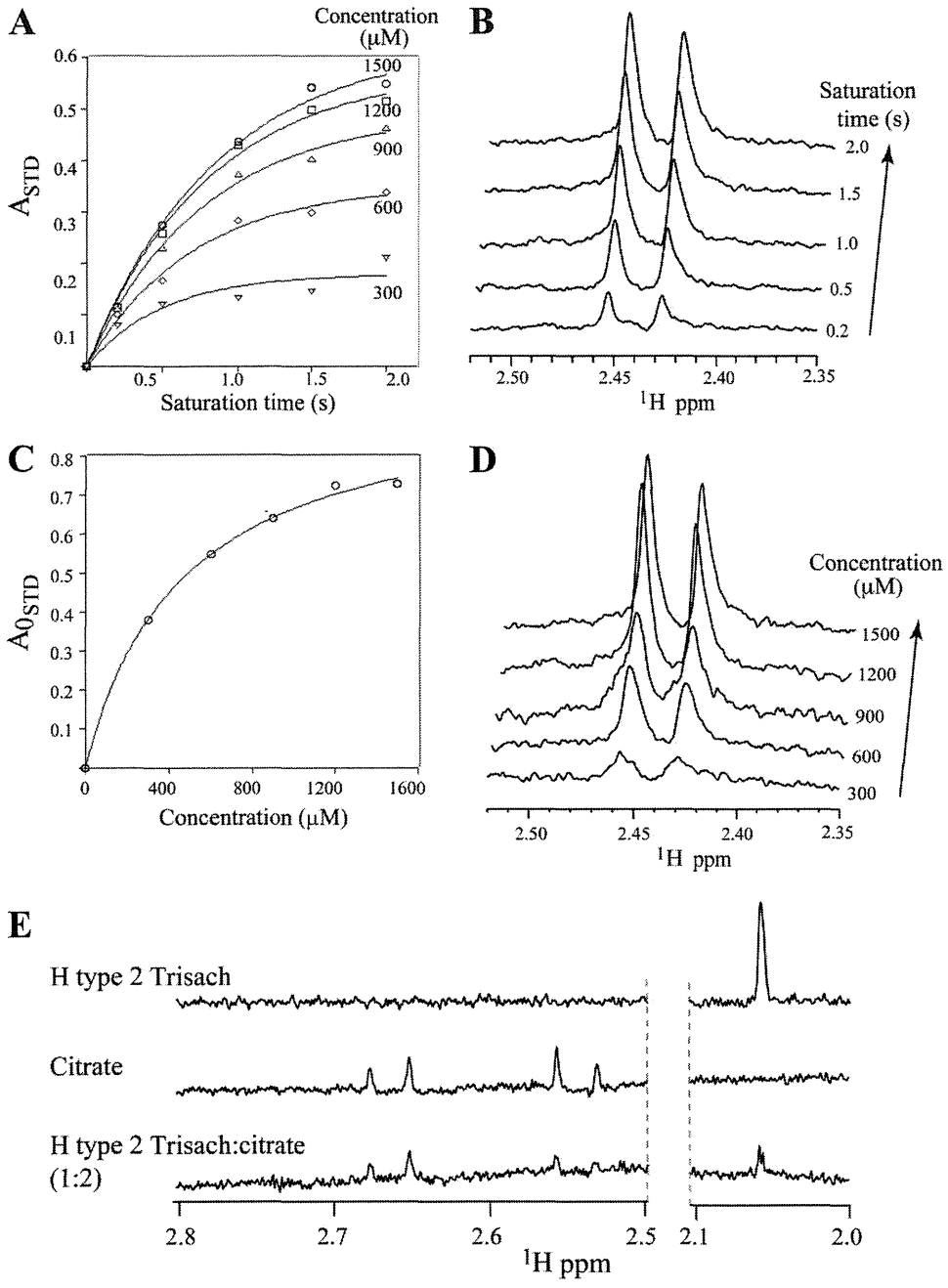


FIG 4 Binding affinity of citrate and HBGAs to GII.10 P domain by STD NMR. Data were used to obtain the $K_D$ for citrate and H type 2 trisaccharide (Trisach) binding to GII.10 P by single-ligand titration STD NMR experiments (2). (A) Effect on STD enhancement (expressed as $A_{STD}$) (34, 37) as a function of saturation time ($t_{sat}$) and ligand concentration; (B) stacked plots of spectra for 1.5 mM citrate as a function of $t_{sat}$ ($y$ axis); (C) Langmuir binding curve used to obtain the $K_D$ from the initial slope of $A_{STD}$ as a function of citrate concentration. (D) Stacked plot of various citrate concentrations ($t_{sat}$, 2 s, 15 $\mu$M protein); (E) competition STD spectra of H type 2 trisaccharide (top), citrate (middle), and 1:2 H type 2 trisaccharide-citrate (0.75:1.5 mM; bottom) used to calculate the $K_i$ of citrate (36).

these amino acid changes, few if any occurred at the fucose-binding site, thus highlighting the common site of vulnerability for GII noroviruses, especially for the pandemic GII.4 variant noroviruses. It is not known if the GI noroviruses will bind citrate given that the GI and GII P domain interactions with HBGAs were different, but since GI.1 P domain interacted with $\alpha$-fucose1-2 and it was reported that the HBGA binding site was conserved among GI noroviruses (12), we suspect that GI noroviruses may also bind citrate, although further structural studies are needed.

Our unexpected finding that citrate and fucose have similar binding modes to the norovirus GII.10 P domain raises the question of whether such citrate mimicry of monosaccharide binding could be a general phenomenon or whether it is spe-

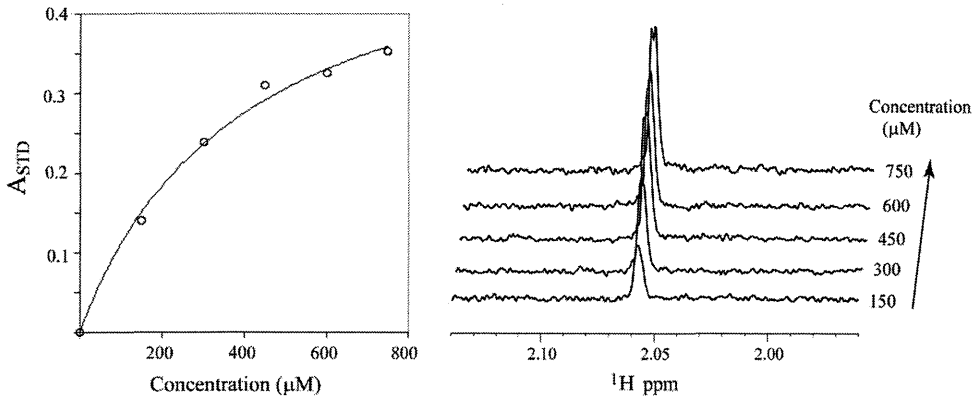


FIG 5 Binding affinity of H type 2 trisaccharide to the GII.10 P domain (left) effect on STD enhancement, expressed as $A_{STD}$, as a function of trisaccharide concentration in the presence of 15 μM GII.10 P domain. $t_{sat}$ = 0.1 s. Curve fitting (described in the text) provides the $K_D$ value. (Right) Stacked STD NMR spectra showing the change in enhancement of the nonoverlapped *N*-acetyl proton signals as a function of increasing concentration of H type 2 trisaccharide (40).

cific to norovirus and other caliciviruses. To investigate this, we performed *in silico* docking studies of citrate against four different fucose-binding proteins (*Anguilla anguilla* agglutinin, *Aleuria aurantia* lectin, *Streptococcus pneumoniae* virulence factor SpGH98, and *Pseudomonas aeruginosa* PA-IIL lectin) and two other saccharide-binding proteins (parainfluenza virus 5 hemagglutinin-neuraminidase and porcine adenovirus type 4 galectin domain), for which fucose or other saccharide-bound crystal structures were available (see Table S1 in the supplemental material). Computational docking analyses reveal different levels of citrate mimicry of monosaccharide binding for other saccharide-binding proteins. For *Anguilla anguilla* agglutinin, citrate, in its predicted binding pose, overlapped with the C-5, C-4, C-3, O-5, O-4, and O-3 atoms of fucose in a similar way to what was observed in the GII.10 P domain (Table S1), while forming hydrogen bonds with the same sets of protein residues as fucose (see Fig. S4 in the supplemental material). Citrate was thus predicted to show a high degree of mimicry to fucose, similarly to our experimental findings for the GII.10 P domain. For the other three fucose-binding proteins, citrate, in its predicted binding poses, did not overlap with the cocrystallized fucose, although it still formed the same sets of polar interactions as the cocrystallized fucose (see Fig. S5 to S7 in the supplemental material). Hence, our docking studies suggest that the mimicry between citrate and fucose binding observed for the GII.10 P domain could be a common, although not universal, phenomenon across other fucose-binding proteins. For all six fucose- and other saccharide-bound proteins for which docking was performed, the predicted citrate binding poses were able to form polar interactions with the same sets of protein residues as the cocrystallized ligand see (Fig. S4 to S9 in the supplemental material), indicating that citrate might be generally useful as a scaffold for designing glycomimetic inhibitors against these and other saccharide-interacting pathogens. Furthermore, a search of the ZINC database (4) revealed that there are more than three thousand compounds with at least 50% similarity to citrate. Thus, *in silico* screening of this database may present a promising approach for identifying small molecules that bind to saccharide-binding proteins. We note, however, that the predicted binding pose of citrate docked to fucose-bound GII.10 P domain had a root mean square deviation (RMSD) of 3.60 Å, while the predicted binding pose of citrate docked to citrate-bound GII.10 P domain with the cocrystallized water molecule had an RMSD of 1.87 Å. This indicates that the resulting docking modes could be error prone. Given that calculating small molecule-receptor binding energies is a difficult and error-prone task (24, 46), ultimately experimental validation would be necessary to confirm the generality of the citrate-saccharide mimicry predicted here.

The STD NMR data provided strong evidence that the integrity of the GII.10 P domain remained unchanged in the presence of different concentrations of citrate buffer and since the pH of the citrate buffer remained more or less the same during the titration, a specific effect of citrate was responsible for the reduction in HBGA attachment. Although the $K_D$ values of citrate and H type 2 trisaccharide for the GII.10 P domain are in the range of 360 to 490 μM, these relatively weak affinities are typical for univalent protein-carbohydrate interactions (17, 28). Given that 90 copies of dimeric P domains are present on norovirus capsid, it is plausible that a multivalent version of citrate- or fucose-like ligands would greatly enhance affinities and provide a starting point for norovirus inhibitors. Indeed, Rademacher et al. show that multivalent fucose-like compounds have increased avidity over their univalent counterparts (44).

In conclusion, we have described the structural basis by which citrate binds to the HBGA binding site of the norovirus GII.10 P domain and can in turn inhibit HBGA binding. Natural compounds, such as juice from lemons and limes, which contain ~300 mM citric acid (42), may already reduce or inhibit norovirus infections, as suggested by a number of recent studies (23, 48–50, 54). In regard to this, it is tempting to speculate that a few drops of lemon juice with one's oysters might reduce norovirus infection. Epidemiological studies on the ingestion of foods high in citrate and norovirus infection may be illuminating, as may be correlations with related glycomimetics—e.g., with ascorbic acid (vitamin C). Controlled possibly volunteer studies should also provide an accurate assessment of norovirus inhibition. Additional compound screening will likely be required to identify a universal norovirus inhibitor with high potency and broad reactivity, and the structural basis for norovirus interaction with citrate as revealed here may be helpful in such efforts.

## ACKNOWLEDGMENTS

We thank members of the Structural Biology Section and Structural Bioinformatics Core at the NIH Vaccine Research Center for comments on the manuscript and J. Stuckey for assistance with figures.

G.S.H., S.H., K.K., C.A.B., and P.D.K. designed the research, G.S.H., S.H., J.S.M., and T.S. performed the research, G.S.H., S.H., J.S.M., G.-Y.C., I.G., C.A.B., and P.D.K. analyzed the data, and G.S.H., S.H., G.-Y.C., I.G., C.A.B., and P.D.K. wrote the paper, on which all authors commented.

Support for this work was provided by the Intramural Research Program of the National Institutes of Health (NIDDK, C.A.B; NIAID, P.D.K); the Intramural AIDS Targeted Antiviral Program, Office of the Director, NIH (C.A.B.); a grant from The Japan Health Science Foundation; and by grants from the Ministry of Health, Labor, and Welfare of Japan. Use of sector 22 (Southeast Region Collaborative Access team) at the Advanced Photon Source was supported by the U.S. Department of Energy, Basic Energy Sciences, Office of Science, under contract no. W-31-109-Eng-38.

## REFERENCES

1. **Adams PD, et al.** 2010. PHENIX: a comprehensive Python-based system for macromolecular structure solution. Acta Crystallogr. D. Biol. Crystallogr. **66**:213–221.
2. **Angulo J, Enriquez-Navas PM, Nieto PM.** 2010. Ligand-receptor binding affinities from saturation transfer difference (STD) NMR spectroscopy: the binding isotherm of STD initial growth rates. Chemistry **16**:7803–7812.
3. **Ausar SF, Foubert TR, Hudson MH, Vedvick TS, Middaugh CR.** 2006. Conformational stability and disassembly of Norwalk virus-like particles. Effect of pH and temperature. J. Biol. Chem. **281**:19478–19488.
4. **Berman HM, et al.** 2000. The Protein Data Bank. Nucleic Acids Res. **28**:235–242.
5. **Bianchet MA, Odom EW, Vasta GR, Amzel LM.** 2002. A novel fucose recognition fold involved in innate immunity. Nat. Struct. Biol. **9**:628–634.
6. **Bok K, et al.** 2009. Evolutionary dynamics of GII. 4 noroviruses over a 34-year period. J. Virol. **83**:11890–11901.
7. **Boraston AB, Wang D, Burke RD.** 2006. Blood group antigen recognition by a Streptococcus pneumoniae virulence factor. J. Biol. Chem. **281**: 35263–35271.
8. **Bu W, et al.** 2008. Structural basis for the receptor binding specificity of Norwalk virus. J. Virol. **82**:5340–5347.
9. **Bull RA, Tu ET, McIver CJ, Rawlinson WD, White PA.** 2006. Emergence of a new norovirus genotype II.4 variant associated with global outbreaks of gastroenteritis. J. Clin. Microbiol. **44**:327–333.
10. **Bull RA, White PA.** 2011. Mechanisms of GII.4 norovirus evolution. Trends Microbiol. **19**:233–240.
11. **Cao S, et al.** 2007. Structural basis for the recognition of blood group trisaccharides by norovirus. J. Virol. **81**:5949–5957.
12. **Choi JM, Hutson AM, Estes MK, Prasad BV.** 2008. Atomic resolution structural characterization of recognition of histo-blood group antigens by Norwalk virus. Proc. Natl. Acad. Sci. U. S. A. **105**:9175–9180.
13. **Collaborative Computational Project N.** 1994. The CCP4 suite: programs for protein crystallography. Acta Crystallogr. D. Biol. Crystallogr. **50**:760–763.
14. **De Jong JC, Rimmelzwaan GF, Fouchier RA, Osterhaus AD.** 2000. Influenza virus: a master of metamorphosis. J. Infect. **40**:218–228.
15. **de Rougemont A, et al.** 2011. Qualitative and quantitative analysis of the binding of GII.4 norovirus variants onto human blood group antigens. J. Virol. **85**:4057–4070.
16. **Emsley P, Lohkamp B, Scott WG, Cowtan K.** 2010. Features and development of Coot. Acta Crystallogr. D. Biol. Crystallogr. **66**:486–501.
17. **Fang M, Agha S, Lee R, Culpepper-Morgan J, D'Souza A.** 2000. Perforation of jejunal diverticulum: case report and review of literature. Conn. Med. **64**:7–10.
18. **Feng X, Jiang X.** 2006. Library screen for inhibitors targeting norovirus binding to their histo-blood group antigen receptors. Antimicrob. Agents Chemother. **51**:324–331.
19. **Fujihashi M, Peapus DH, Kamiya N, Nagata Y, Miki K.** 2003. Crystal structure of fucose-specific lectin from Aleuria aurantia binding ligands at three of its five sugar recognition sites. Biochemistry **42**:11093–11099.
20. **Guardado-Calvo P, et al.** 2010. Crystallographic structure of porcine adenovirus type 4 fiber head and galectin domains. J. Virol. **84**: 10558–10568.
21. **Hansman GS, et al.** 2011. Crystal structures of GII.10 and GII.12 norovirus protruding domains in complex with histo-blood group antigens reveal details for a potential site of vulnerability. J. Virol. **85**:6687–6701.
22. **Hansman GS, et al.** 2004. Detection of norovirus and sapovirus infection among children with gastroenteritis in Ho Chi Minh City, Vietnam. Arch. Virol. **149**:1673–1688.
23. **Horm KM, D'Souza DH.** 2011. Survival of human norovirus surrogates in milk, orange, and pomegranate juice, and juice blends at refrigeration (4 degrees C). Food Microbiol. **28**:1054–1061.
24. **Huey R, Morris GM, Olson AJ, Goodsell DS.** 2007. A semiempirical free energy force field with charge-based desolvation. J. Comput. Chem. **28**: 1145–1152.
25. **Jiang X, Wang M, Graham DY, Estes MK.** 1992. Expression, self-assembly, and antigenicity of the Norwalk virus capsid protein. J. Virol. **66**:6527–6532.
26. **Kageyama T, et al.** 2004. Coexistence of multiple genotypes, including newly identified genotypes, in outbreaks of gastroenteritis due to norovirus in Japan. J. Clin. Microbiol. **42**:2988–2995.
27. **Kapikian AZ, et al.** 1972. Visualization by immune electron microscopy of a 27-nm particle associated with acute infectious nonbacterial gastroenteritis. J. Virol. **10**:1075–1081.
28. **Kiessling LL, Young T, Gruber TD, Mortell KH.** 2008. Glycoscience 12. **4**:2483–2523.
29. **Levin SA, Dushoff J, Plotkin JB.** 2004. Evolution and persistence of influenza A and other diseases. Math. Biosci. **188**:17–28.
30. **Lindesmith LC, Donaldson EF, Baric RS.** 2011. Norovirus GII.4 strain antigenic variation. J. Virol. **85**:231–242.
31. **Lindesmith LC, et al.** 2008. Mechanisms of GII.4 norovirus persistence in human populations. PLoS Med. **5**:e31.
32. **Marionneau S, et al.** 2001. ABH and Lewis histo-blood group antigens, a model for the meaning of oligosaccharide diversity in the face of a changing world. Biochimie **83**:565–573.
33. **Marotte K, et al.** 2007. X-ray structures and thermodynamics of the interaction of PA-IIL from Pseudomonas aeruginosa with disaccharide derivatives. Chem. Med. Chem. **2**:1328–1338.
34. **Mayer M, Meyer B.** 2001. Group epitope mapping by saturation transfer difference NMR to identify segments of a ligand in direct contact with a protein receptor. J. Am. Chem. Soc. **123**:6108–6117.
35. **McCoy AJ, et al.** 2007. Phaser crystallographic software. J. Appl. Crystallogr. **40**:658–674.
36. **Meinecke R, Meyer B.** 2001. Determination of the binding specificity of an integral membrane protein by saturation transfer difference NMR: RGD peptide ligands binding to integrin alphaIIbbeta3. J. Med. Chem. **44**:3059–3065.
37. **Meyer B, Peters T.** 2003. NMR spectroscopy techniques for screening and identifying ligand binding to protein receptors. Angew Chem. Int. ed. Engl. **42**:864–890.
38. **Mitchell EP, et al.** 2005. High affinity fucose binding of Pseudomonas aeruginosa lectin PA-IIL: 1.0 A resolution crystal structure of the complex combined with thermodynamics and computational chemistry approaches. Proteins **58**:735–746.
39. **Morris GM, et al.** 1998. Automated docking using a Lamarckian genetic algorithm and empirical binding free energy function. J. Comput. Chem. **19**:1639–1662.
40. **Neffe AT, Bilang M, Meyer B.** 2006. Synthesis and optimization of peptidomimetics as HIV entry inhibitors against the receptor protein CD4 using STD NMR and ligand docking. Org. Biomol. Chem. **4**:3259–3267.
41. **Otwinowski Z, Minor W.** 1997. Processing of X-ray diffraction data collected in oscillation mode. Methods Enzymol. **276**:307–326.
42. **Penniston KL, Nakada SY, Holmes RP, Assimos DG.** 2008. Quantitative assessment of citric acid in lemon juice, lime juice, and commercially-available fruit juice products. J. Endourol. **22**:567–570.
43. **Prasad BV, et al.** 1999. X-ray crystallographic structure of the Norwalk virus capsid. Science **286**:287–290.
44. **Rademacher C, et al.** 2011. Targeting norovirus infection-multivalent entry inhibitor design based on NMR experiments. Chemistry **17**: 7442–7453.
45. **Rademacher C, Krishna NR, Palcic M, Parra F, Peters T.** 2008. NMR experiments reveal the molecular basis of receptor recognition by a calicivirus. J. Am. Chem. Soc. **130**:3669–3675.

46. **Shoichet BK.** 2004. Virtual screening of chemical libraries. Nature **432**: 862–865.
47. **Siebenga JJ, et al.** 2010. Phylodynamic reconstruction reveals norovirus GII.4 epidemic expansions and their molecular determinants. PLoS Pathog. **6**:e1000884.
48. **Su X, Howell AB, D'Souza DH.** 2010. Antiviral effects of cranberry juice and cranberry proanthocyanidins on foodborne viral surrogates—a time dependence study in vitro. Food Microbiol. **27**:985–991.
49. **Su X, Howell AB, D'Souza DH.** 2010. The effect of cranberry juice and cranberry proanthocyanidins on the infectivity of human enteric viral surrogates. Food Microbiol. **27**:535–540.
50. **Su X, Sangster MY, D'Souza DH.** 2010. In vitro effects of pomegranate juice and pomegranate polyphenols on foodborne viral surrogates. Foodborne Pathog. Dis. **7**:1473–1479.
51. **Tan M, Hegde RS, Jiang X.** 2004. The P domain of norovirus capsid protein forms dimer and binds to histo-blood group antigen receptors. J. Virol. **78**:6233–6242.
52. **Tan M, et al.** 2009. Conservation of carbohydrate binding interfaces: evidence of human HBGA selection in norovirus evolution. PLoS One **4**:e5058.
53. Reference deleted.
54. **Whitehead K, McCue KA.** 2010. Virucidal efficacy of disinfectant actives against feline calicivirus, a surrogate for norovirus, in a short contact time. Am. J. Infect. Control. **38**:26–30.
55. Reference deleted.
56. **Yuan P, et al.** 2005. Structural studies of the parainfluenza virus 5 hemagglutinin-neuraminidase tetramer in complex with its receptor, sialyllactose. Structure **13**:803–815.
57. **Zheng DP, et al.** 2006. Norovirus classification and proposed strain nomenclature. Virology **346**:312–323.

Arch Virol
DOI 10.1007/s00705-012-1387-7

BRIEF REPORT

# A confirmation of sapovirus re-infection gastroenteritis cases with different genogroups and genetic shifts in the evolving sapovirus genotypes, 2002-2011

**Seiya Harada · Tomoichiro Oka · Eisuke Tokuoka · Naoko Kiyota · Koichi Nishimura · Yasushi Shimada · Takehiko Ueno · Shigeru Ikezawa · Takaji Wakita · Qiuhong Wang · Linda J. Saif · Kazuhiko Katayama**

Received: 10 April 2012 / Accepted: 12 May 2012


**Abstract** Sapovirus (SaV) is an important pathogen that causes acute gastroenteritis in humans. Human SaV is highly diverse genetically and is classified into multiple genogroups and genotypes. At present, there is no clear evidence for gastroenteritis cases caused by re-infection with SaV. We found that two individuals were sequentially infected with SaVs of two different genogroups and had gastroenteritis after each infection, although in one of the subsequent cases, both SaV and norovirus were detected. We also found a genetic shift in SaVs from gastroenteritis outpatients in the same geographical location. Our results suggest that protective immunity may be at least genogroup-specific for SaV.

**Keywords** Sapovirus · Gastroenteritis · Genotyping · Re-infection

S. Harada and T. Oka contributed equally to this study.

S. Harada · E. Tokuoka · N. Kiyota · K. Nishimura
Kumamoto Prefectural Institute of Public Health and Environmental Science, Kumamoto, Japan

T. Oka (✉) · T. Wakita · K. Katayama
Department of Virology II, National Institute of Infectious Diseases, Gakuen 4-7-1, Musashi-murayama, Tokyo 208-0011, Japan
e-mail: oka-t@nih.go.jp

T. Oka · Q. Wang · L. J. Saif
Department of Veterinary Preventive Medicine, Food Animal Health Research Program, Ohio Agricultural Research and Development Center, The Ohio State University, Wooster, OH, USA

Y. Shimada
Shimada Children's Clinic, Kumamoto, Japan

T. Ueno
Ueno Pediatric Clinic, Kumamoto, Japan

S. Ikezawa
Ikezawa Children's Clinic, Kumamoto, Japan

Sapovirus (SaV), a member of the family *Caliciviridae*, is an important pathogen that causes acute gastroenteritis [1, 2, 5, 8, 10, 11, 13, 14, 20–25]. The SaV genome is a single-stranded 7.5-kb RNA molecule of positive polarity. SaV strains are highly diverse, especially in the capsid-encoding region [16], and are divided into at least five genogroups (GI to GV): Viruses belonging to GI, GII, GIV, and GV infect humans, and those belonging to GIII infect pigs [3, 18]. Based on the complete nucleotide sequences of the capsid gene, we have classified human SaVs into 16 genotypes (GI.1-7, GII.1-7, GIV, and GV)[18]. To date, there is no clear evidence for cases of gastroenteritis due to re-infection with SaV.

Previously, we identified 81 SaVs from outpatients with acute gastroenteritis in three pediatric clinics during 2002-2007 [8]. However, genotype analysis has not been performed with those samples. In this study, we detected 58 SaVs from the same clinics from 2008 to 2011 and genotyped all 139 SaVs isolated from 2002 to 2011. For the first time, we have identified cases of gastroenteritis due to re-infection with SaVs belonging to different genogroups. The GIV SaVs, which emerged in 2007, were not detected between 2008 and 2011, and the major genotype changed to GII.3 in 2008.

Stool specimens were collected from 728 patients with acute gastrointestinal symptoms at three pediatric clinics in Kumamoto Prefecture, Japan, from January 2008 to March 2011. Acute gastroenteritis was defined as a case in which

Published online: 08 July 2012

the patient exhibits one or more of the following symptoms: vomiting, abdominal pain, and diarrhea. Specimens were collected during the symptomatic period, transported to the Kumamoto Prefectural Institute of Public Health and Environmental Science, and stored at −80°C until use. Viral nucleic acid extraction, cDNA synthesis, and PCR screening for SaV with the primers SaV124F, SaV1F, SaV5F, and SaV1245R[16] were performed as described [8]. For SaV-positive specimens, genogroup-specific PCR with primers SV-F13, SV-F14, SV-G1-R, SV-G2-R, SV-G4-R, and SV-G5-R [20] and nested PCR with primers SV-F13, SV-F14, SV-R13, and SV-R14 for the first PCR and with primers SV-F22 and SV-R2 or SV-F22, SV-R13, and SV-R14 for the second PCR [20] were performed as described [8]. PCR products corresponding to the partial SaV capsid-encoding region were purified and sequenced as described [8, 9]. SaV was detected in 58 (8.0 %) of 728 stool specimens collected from January 2008 to March 2011. All of these 58 specimens were successfully amplified in combination with a genogroup-specific PCR or nested PCR; 55 (94.8 %) and 54 (93.1 %) were positive by genogroup-specific PCR and nested PCR, respectively. These results demonstrate the efficiency of the SaV screening PCR assays used in this study. Nucleotide sequences for the 58 SaV strains that were newly detected during 2008 to 2011 were deposited in GenBank/EMBL/DDBJ under accession numbers AB689798-AB689855.

In total, 139 SaV strains were detected from 2002 to 2011 (81 sequenced in the previous study [8], and 58 newly identified and sequenced in this study) and were genotyped using phylogenetic analysis based on approximately 270 nucleotides of the partial capsid encoding region with reference strain sequences corresponding to the 16 genotypes (GI.1-7, GII.1-7, GIV, and GV) as described [18]. To investigate possible SaV re-infection cases, clinical records of the 139 SaV-positive patients were analyzed by the medical doctors of the three clinics. Stool specimens from the patients from whom SaVs were detected twice during the study period were further screened for enteric pathogens including norovirus (NoV), rotavirus, enteric adenovirus, astrovirus, kobuvirus, enterovirus, *Campylobacter*, *Escherichia coli* causing diarrhea, *Salmonella*, and *Shigella*. The sapovirus RNA load was determined by real-time PCR as described previously [8, 16].

As shown in Table 1, three children (patients A, B, and C) were positive for SaV twice during the study period. Patient A was positive for GI.1 SaV ($1.50 \times 10^9$ copies/gram of stool) in January 2007, and GIV SaV ($1.07 \times 10^{11}$ copies/gram stool) in November 2007. Patient B was positive for GI.1 SaV ($1.19 \times 10^8$ copies/gram stool) in December 2006, and both GII.3 SaV ($1.00 \times 10^6$ copies/gram stool) and NoV GII ($7.63 \times 10^9$ copies/gram stool) were detected in March 2009. Patient C was positive for GII.3 SaV ($1.56 \times 10^{11}$ copies/gram stool) at the first visit, and both GII.3 SaV ($5.60 \times 10^6$ copies/gram stool) and GII NoV ($5.05 \times 10^9$ copies/gram stool) were detected 18 days after the first visit (Table 1). Rotavirus, enteric adenovirus, astrovirus, kobuvirus, enterovirus, *Campylobacter, Escherichia coli* causing diarrhea, *Salmonella*, and *Shigella* were not detected in these three patients.

In this study, we detected at least two cases of re-infection with SaV of different genogroups 10 months (patient A) and 27 months (patient B) after their first visit to the clinic. Patient A was clearly a SaV re-infection gastroenteritis case, whereas SaV and/or NoV likely contributed to the diarrhea in the second visit in the case of

**Table 1** Description of three gastroenteritis patients in whom sapovirus (SaV) was detected twice

| Patient | Visit to clinic | Date of collection of stool specimen | SaV genotype | SaV copies/g stool[a] | Other pathogens[b] | NoV copies/g stool[c] | Clinical symptoms | Age | Sex |
|---|---|---|---|---|---|---|---|---|---|
| A | 1st | 2007 Jan 23 | GI.1 | $1.50\times10^9$ | –[d] | –[d] | Diarrhea, vomiting, abdominal pain | 6 y 9 mo | F |
| | 2nd | 2007 Nov 20 | GIV | $1.07\times10^{11}$ | –[d] | –[d] | Diarrhea, vomiting, abdominal pain | | |
| B | 1st | 2006 Dec 14 | GI.1 | $1.19\times10^8$ | –[d] | –[d] | Diarrhea | 2 y 7 mo | M |
| | 2nd | 2009 Mar 3 | GII.3 | $1.00\times10^6$ | NoV GII | $7.63\times10^9$ | Diarrhea | | |
| C | 1st | 2008 Nov 7 | GII.3 | $1.56\times10^{11}$ | –[d] | –[d] | Bloody diarrhea | 3 y 8 mo | F |
| | 2nd | 2008 Nov 25 | GII.3 | $5.60\times10^6$ | NoV GII | $5.05\times10^9$ | Vomiting | | |

[a] Quantitative SaV real-time RT-PCR was performed as described previously (ref 8, 16)

[b] Negative for rotavirus, enteric adenovirus, astrovirus, kobuvirus, enterovirus, *Campylobacter*, *Escherichia coli* causing diarrhea, *Salmonella*, and *Shigella*, tested as described previously (ref 8)

[c] Quantitative norovirus (NoV) real-time RT-PCR was performed as previously described (ref 8)

[d] Negative for NoV and other gastroenteritis pathogens tested as listed above

**Table 2** Sapovirus genotypes in gastroenteritis outpatients at three pediatric clinics in the same area between June 2002 and March 2011

| | Jan | Feb | Mar | Apr | May | Jun | Jul | Aug | Sep | Oct | Nov | Dec | Total number of SaV cases in each year |
|---|---|---|---|---|---|---|---|---|---|---|---|---|---|
| 2002 | NA | NA | NA | NA | NA | | | | | | | GI.1 (2) | 2 |
| 2003 | | GI.1 (1)<br>GII.1 (1)<br>GII.2 (1) | GII.4 (1) | GII.2 (1) | | | | | | | | GII.3 (2) | 7 |
| 2004 | | | | | | | | | | | | GV (2) | 2 |
| 2005 | GI.1 (1) | | | | | | | | | | GI.1 (1)<br>GI.6 (1) | GI.1 (1)<br>GI.6 (3) | 7 |
| 2006 | | | | | | | | | GI.1 (1) | | GI.1 (1)<br>GV (1) | GI.1 (4)<br>GII.1 (3)<br>GII.2 (1) | 11 |
| 2007 | GI.1 (1) | | | | | | | | GIV(1) | GIV(11) | GIV (29) | GIV (10) | 52 |
| **2008** | | **GII.7 (1)** | | **GII.3 (1)**<br>**GV (1)** | **GII.3 (2)** | **GII.3 (1)** | | | | **GII.3 (1)** | **GII.3 (3)** | **GII.3 (1)** | **11** |
| **2009** | **GI.1 (1)**<br>**GII.1 (1)**<br>**GII.3 (1)** | **GI.3 (2)**<br>**GII.1 (3)**<br>**GII.3 (1)** | **GII.3 (5)** | **GI.1 (1)**<br>**GII.3 (2)** | **GII.3 (1)** | | | | | **GII.3 (3)** | **GII.3 (1)** | | **22** |
| **2010** | | **GI.1 (1)** | **GI.1 (4)** | **GI.1 (4)**<br>**GII.3 (1)** | **GI.2 (3)** | **GI.1 (1)**<br>**GII.1 (1)** | **GII.2 (1)** | | | | **GII.3 (2)** | **GI.1 (1)**<br>**GII.1 (1)**<br>**GII.3 (1)**<br>**GV (1)** | **22** |
| **2011** | | | **GII.1 (2)**<br>**GV (1)** | **NA** | **NA** | **NA** | **NA** | **NA** | **NA** | **NA** | **NA** | **NA** | **3** |
| Total numbers of SaV in each month | 5 | 11 | 13 | 11 | 6 | 3 | 1 | 0 | 2 | 15 | 39 | 33 | |

The 58 strains detected from 2008 to 2011 are indicated in bold

Nucleotide sequences for the 81 SaV strains detected from 2002 to 2007 were deposited in GenBank/EMBL/DDBJ under accession numbers AB429079-AB429159 (ref 8)

Nucleotide sequences for the 58 SaV strains detected from 2008 to 2011 were deposited in GenBank/EMBL/DDBJ under accession numbers AB689798-AB689855

Genotype numbers are according to the classfication scheme of Oka et al. (ref 18)

The numbers detected are indicated in parentheses

*NA* no samples were available